

SELMA: How do airless bodies interact with space environment?

1 **SELMA mission: How do airless bodies interact**
2 **with space environment? The Moon as an accessible**
3 **laboratory**

4

5 Yoshifumi Futaana, Stas Barabash, Martin Wieser

6 *Swedish Institute of Space Physics, Box 812, Kiruna SE 98128, Sweden.*

7 *E-mail: futaana@irf.se*

8 Peter Wurz

9 *University of Bern, Bern, Switzerland*

10 Dana Hurley

11 *The Johns Hopkins University Applied Physics Laboratory, Laurel, USA*

12 Mihaly Horányi

13 *Laboratory for Atmospheric and Space Physics, University of Colorado, USA*

14 Urs Mall

15 *Max Planck Institute for Solar System Research, Göttingen, Germany*

16 Nicolas Andre

17 *IRAP- Université de Toulouse, CNRS, France*

18 Nickolay Ivchenko

19 *KTH Royal Institute of Technology, Stockholm, Sweden*

20 Jürgen Oberst

21 *German Aerospace Center, Berlin, Germany*

22 Kurt Retherford

23 *Southwest Research Institute, San Antonio, USA*

24 Andrew Coates

25 *Mullard Space Science Laboratory, University College London, London, UK*

26 Adam Masters

27 *Imperial College London, London, UK*

28 Jan-Erik Wahlund

29 *Swedish Institute of Space Physics, Uppsala, Sweden*

30 Esa Kallio

31 *Aalto University, Helsinki, Finland*

32 and the SELMA proposal team.

33

34 **Keyword: Moon exploration, volatile, water, mini-magnetosphere, dust, permanently**
35 **shadowed crater**

36 **Abstract:**

37 The Moon is an archetypal atmosphere-less celestial body in the Solar System. For such bodies,
38 the environments are characterized by complex interaction among the space plasma, tenuous
39 neutral gas, dust and the outermost layer of the surface. Here we propose the SELMA mission
40 (Surface, Environment, and Lunar Magnetic Anomalies) to study how airless bodies interact with
41 space environment. SELMA uses a unique combination of remote sensing via ultraviolet and
42 infrared wavelengths, and energetic neutral atom imaging, as well as in situ measurements of
43 exospheric gas, plasma, and dust at the Moon. After observations in a lunar orbit for one year,
44 SELMA will conduct an impact experiment to investigate volatile content in the soil of the
45 permanently shadowed area of the Shackleton crater. SELMA also carries an impact probe to
46 sound the Reiner-Gamma mini-magnetosphere and its interaction with the lunar regolith from the
47 SELMA orbit down to the surface. SELMA was proposed to the European Space Agency as a
48 medium-class mission (M5) in October 2016. Research on the SELMA scientific themes is of
49 importance for fundamental planetary sciences and for our general understanding of how the
50 Solar System works. In addition, SELMA outcomes will contribute to future lunar explorations
51 through qualitative characterization of the lunar environment and, in particular, investigation of
52 the presence of water in the lunar soil, as a valuable resource to harvest from the lunar regolith.

53 **1 Introduction**

54 The Moon, Phobos, Deimos, and the majority of planetary satellites, Mercury, dwarf planets, and
55 asteroids do not possess atmospheres. Solar radiation, space plasmas, meteoroids, and dust
56 directly access the surface, changing its properties (called space weathering) and resulting in an
57 environment where four main components, plasma, neutral gas, dust, and the outermost layer of
58 the surface interact with each other in a very complex way. In order to investigate these
59 interactions, we have designed a new-generation lunar mission, SELMA (Surface, Environment,
60 and Lunar Magnetic Anomalies).

61 The mission SELMA was proposed in response to *the call for a Medium-size Mission*
62 *Opportunity in European Space Agency's (ESA) science program (M5)*. SELMA is a mission in
63 the frame of the Cosmic Vision themes “1. What are the conditions for planet formation and the
64 emergence of life?” and “2. How does the Solar System work?” (*Cosmic Vision, 2005*). SELMA
65 addresses the Cosmic Vision topics “1.3 Life and habitability in the Solar System” and “2.3
66 Asteroids and other small bodies”.

67 The science question of SELMA is "How do airless bodies interact with space environment?".
68 SELMA studies the Moon, an archetypal atmosphere-less celestial body in the Solar System.
69 SELMA studies water, one of the main ingredients for the life as we know it. SELMA will reveal
70 the mechanisms of the water/hydroxyl formation on regolith-covered surfaces. While such bodies
71 hardly can or could have been habitable, general studies how water is created, transported, stored,
72 and escapes are an important contribution to understanding the fate of water in the solar system.
73 SELMA also studies how airless bodies and small magnetic structures (magnetic anomalies)
74 interact with the solar wind plasma, how surface bounded exospheres are created and maintained,
75 and how the dust environment works; details of the scientific objectives are described in Section
76 2. All these results are of fundamental importance for planetary science and can be applicable
77 throughout the solar system including the moons of Jupiter and Saturn, asteroids and dwarf
78 planets.

79 In order to realize the science objectives, SELMA comprises of the SELMA orbiter, SELMA
80 impact probe for Magnetic Anomaly (SIP-MA), passive impactor (10 kg copper sphere), and a

SELMA: How do airless bodies interact with space environment?

81 relay CubeSat (RCS). The SELMA orbiter and SIP-MA host scientific instruments. The SELMA
82 orbiter carries four remote sensing instruments and seven in-situ instruments. SIM-MA is
83 equipped with four scientific instruments. The SELMA mission's lifetime is 15 months. The
84 launch time is flexible, while the proposed SELMA mission complies with the requirement of
85 ESA's M5 mission time line, i.e., aiming at 2029. The SELMA orbiter is inserted into a lunar
86 polar orbit, nominally with a pericenter at 30 km and an apocenter at 200 km above the surface,
87 for collecting the scientific data for the whole mission period. Two different measurement
88 campaigns are conducted. An impact probe experiment using SIP-MA to investigate the lunar
89 mini-magnetosphere is done 6 months after the launch; while the timing is flexible. The
90 opportunity for SIP-MA is once a month. The second experiment will be done at the end of the
91 mission: A passive impactor will be released aiming at a permanently shadowed region (the
92 Shackleton crater is the baseline) to create an impact plume, which will be measured both
93 remotely and locally by the SELMA orbiter. The SELMA orbiter chases the passive impactor
94 along almost the identical orbit with a full science operation, and it crashes to the closer location
95 to the passive impactor. Details of the mission description and instrumentation are described in
96 Sections 3 and 4.

97 SELMA uses a unique combination of remote sensing via ultraviolet and infrared wavelengths
98 and energetic neutral atom imaging, as well as in situ measurements of exospheric gas, plasma
99 and dust to investigate the complex interaction of surface-space environments. Uniqueness of the
100 SELMA mission is coordination of science and instrumentation throughout the mission; i.e., the
101 mission design, system and instrument development, science operation, and data exploitation.
102 Previous lunar missions have addressed only a part of the interaction. For example, the LADEE
103 mission focused exosphere and dust, Kaguya was for surface and plasma, ARTEMIS is for
104 plasma, and LRO is for surface and exosphere. LCROSS did an impact experiment into a
105 permanently shadowed region, but characterization of the produced plume relied on remote
106 sensing instruments. The SELMA mission is the first mission to investigate the interaction
107 between the surface, exosphere, plasma and dust, using the coordinated measurements.

108 **2 SELMA Science questions**

109 Of the very complex lunar environment interactions, SELMA focuses on four main subjects:
110 water, volatiles cycle, mini-magnetospheres, and dust. The four SELMA key science questions
111 can be described as follows.

112 1. What is the origin of water on the Moon?

113 The surface of non-icy airless bodes is covered with regolith, a layer of loose, heterogeneous
114 material including dust, broken rock, and other related materials (e.g. *Heiken, 1991*). The regolith
115 has been formed by the impact of large and small meteoroids and the steady bombardment of
116 micrometeoroids, which slowly break down surface rocks. One of the most important
117 manifestations of the interaction of the lunar regolith with the solar wind plasma is the formation
118 of OH/H₂O bearing materials in the outermost layer via chemical reactions between oxygen in the
119 regolith's minerals and implanted protons from the solar wind (*Pieters et al. 2009; Sunshine et al.*
120 *2009; Clark, 2009*). The solar wind protons can thus be considered as a one of the sources of
121 water on airless bodies. On the other hand, comets may also have brought substantial amounts of
122 water to planetary bodies during the long period of bombardment, which is another important
123 potential source of water. Answering the question "What is the origin of water on the Moon?" is a
124 key to understanding the water distribution and presence in the Solar System.

125 2. How do the "volatile cycles" on the Moon work?

SELMA: How do airless bodies interact with space environment?

126 The volatiles surrounding airless bodies form a collisionless gas layer, a surface-bounded
127 exosphere (e.g. *Stern, 1999*). At the Moon, the exospheric atoms and molecules originate from
128 the interior, and are kicked off from the regolith grain surface by solar photons and particles, and
129 through micrometeoroids impacts. The release processes are highly variable due to the variability
130 of the solar radiation, impinging particle fluxes, meteoroid fluxes and impact rates, surface
131 mineralogy, temperature, topography and structures, as well as the transient releases of gas from
132 the lunar interior. The exospheric particles do not interact with each other but with the surface
133 and can be redistributed over the whole body. Exospheric particles originating in the hot
134 equatorial regions may get transported to and trapped in the cold polar regions, forming volatile
135 reservoirs there (*Watson et al., 1961*). Some atoms and molecules, especially those of low mass,
136 escape to space due to sufficiently high velocities. Volatiles may also undergo ionization by solar
137 UV radiation, and will be picked-up by the solar wind electric field, and escape the system.
138 Answering the question "How do the "volatiles cycles" work on the Moon?" will reveal the
139 sources and sinks as well as transport processes of the volatiles on airless bodies.

140 3. How do the lunar mini-magnetospheres work?

141 The Moon does not possess a global magnetic dipole field but only local crustal magnetic fields,
142 so-called magnetic anomalies, with field strength of a few 100s nT at the surface (e.g. *Coleman et*
143 *al., 1972; Richmond and Hood, 2008; Tsunawaka et al., 2015*). This field strength is comparable
144 with the weak magnetic dipole field of the Mercury (~195 nT on the equator; e.g. *Ness et al.,*
145 *1974; Anderson et al., 2011*). The magnetic anomalies do affect the local solar wind plasma flow
146 but cannot fully prevent it from reaching the surface (*Vorburger et al., 2012*). Due to the small
147 size of the anomalies, which is between the proton gyroradius and the electron gyroradius, the
148 electrodynamic interaction is inherently kinetic and very complex, being one of the
149 fundamental solar wind interactions in the solar system. These lunar mini-magnetospheres are
150 natural laboratories for studying small-scale plasma interactions in the solar system and the
151 physics of dusty plasma. SELMA will focus on answering the question "How do the lunar mini-
152 magnetospheres work?"

153 4. What is the influence of dust on the lunar environment and surface?

154 Levitating lunar dust, inferred from the Apollo images of horizontal glow (e.g. *McCoy and*
155 *Criswell, 1974; Rennilson and Criswell, 1974*), fascinated scientists, and worried and bewildered
156 engineers and astronauts. Dust was identified as the *number-one* environmental problem on the
157 Moon. However, the physical processes responsible for the mobilization of lofting of the dust
158 particles are not yet fully understood due to complex interaction between the lunar surface and its
159 UV and plasma environment. For example, the continuous interplanetary meteoroid
160 bombardment sustains a permanently present the dust cloud in the exosphere. In addition, the
161 plasma and associated electric fields in the exosphere control the dynamics of the dust particles.
162 Similar processes occur at many astrophysical objects, where dusty plasmas appear frequently;
163 for example, in interstellar molecular clouds, in proto-planetary disks, in cometary tails, planetary
164 rings and surfaces of airless planetary bodies. Therefore, the Moon provides an exceptional
165 testing ground for fundamental research of the physics of complex dusty plasma. SELMA will
166 focus on answering the question "What is the influence of dust on the lunar environment and
167 surface?"

168 From these four overarching science questions, we further derive several science objectives in the
169 following sections. Table 1 summarizes the SELMA science objectives.

170

171 *Table 1: Science objectives of SELMA broken down from the four overarching science questions.*

What is the origin of water on the Moon?

Understand the role of the solar wind in the formation of water bearing materials

Investigate how exospheric gases affect the abundances of water bearing materials and vice versa

Investigate how variable the abundances of OH/H₂O bearing materials are and how the variability is related to the plasma and neutral gas environment

Investigate the solar wind proton balance in the lunar soil

Determine the water content in the regolith of permanently shadowed regions and its isotope composition

How do the “volatile cycles” on the Moon work?

Fully characterize the lunar exosphere

Investigate how the lunar exospheric composition is related to surface illumination conditions and sources due to photon and thermal desorptions

Investigate how the lunar exosphere composition is related to the plasma environment and sources due to surface sputtering

Investigate how the lunar exosphere composition is related to impact events and sources due to impact vaporization

Establish the sinks of the lunar exosphere

How do the lunar mini-magnetospheres work?

Establish the structure and topology of the magnetic field at the surface

Establish the mechanisms creating small-scale plasma depletions and deceleration of electrons and ions.

Investigate how small scale magnetic structures affect the solar wind on the global scale

Investigate how the properties of mini-magnetospheres vary with solar wind conditions

Investigate long-term local effects of magnetic anomalies on the surface

What is the influence of dust on the lunar environment and surface?

Fully characterize the lunar dust environment

Investigate how the impact events affect the lunar dust environments

Investigate how plasma effects result in lofting the lunar plasma

172

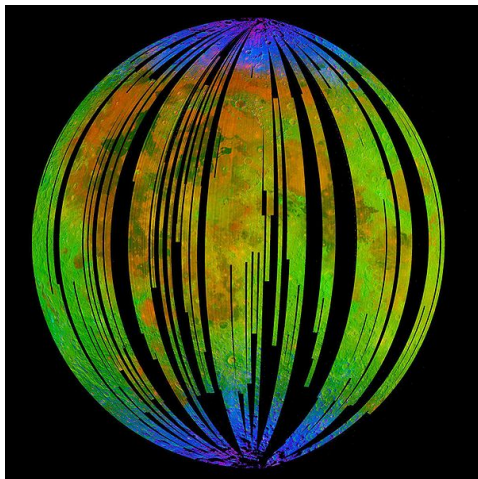
173 **2.1 What is the origin of water on the Moon?**

174 The existence of water on the lunar surface was debated for half a century. *Watson et al. (1961)*
175 contested the previously common assumption that the Moon was completely dry. They
176 considered the possibility of water in its frozen form being accumulated in permanently
177 shadowed regions (cold traps) and calculated very low evaporation rates of ice, concluding that
178 the cold traps should be able to retain water on geological timescales. A long series of theoretical

SELMA: How do airless bodies interact with space environment?

179 studies were thereafter conducted, adding various possible source and loss mechanisms, with
180 differing conclusions (e.g., *Arnold, 1979; Lanzerotti et al., 1981; Hodges, 2002; Cocks et al.,*
181 *2002; Crider and Vondrak, 2003*).

182 Recent missions established that the lunar soil contains hydrogen-rich materials although the
183 exact chemical composition (H/OH/H₂O, ice) is not known. The neutron spectrometer onboard
184 Lunar Prospector (LP) observed a depletion of epithermal neutrons in the polar regions, which
185 was interpreted as the presence of hydrogen-rich materials in the form of water inside the
186 permanently shadowed areas (*Feldman et al., 1998*). The neutron spectrometer on Lunar
187 Reconnaissance Orbiter (LRO) showed that depletions of the epithermal neutrons do not always
188 coincide with the permanently shadowed regions but may also occur in illuminated craters too
189 (*Mitrofanov et al., 2010*). Spectroscopic observations in the near-infrared (NIR) range of the
190 OH/H₂O absorption band (2.7–3.3 μm) on the lunar surface conducted by M3 (Moon Mineral
191 Mapper) onboard Chandrayaan-1 showed that water ice and/or hydroxyl exist in the lunar
192 regolith (*Pieters et al., 2009*; Figure 1). Similar features in the infrared spectra were found in the
193 data from Cassini VIMS (*Clark, 2009*) and HRI-IR spectrometer on Deep Impact (*Sunshine et al.,*
194 *2009*). Phobos and Deimos also exhibit similar signatures in the NIR absorption band (e.g.
195 *Freeman et al., 2014*).



196
197 *Figure 1: Three-color composite image of reflected near-infrared radiation from the Sun as*
198 *obtained by M3. Blue shows the signature of water and hydroxyl molecules as seen by a highly*
199 *diagnostic absorption of infrared light with a wavelength of 3 μm. Green shows the brightness of*
200 *the surface as measured by reflected infrared radiation from the Sun with a wavelength of 2.4-μm,*
201 *and red shows an iron-bearing mineral called pyroxene, detected by absorption of infrared light*
202 *at 2.0-μm. The figure is from Pieters et al. (2009).*

203 Currently, two main hypotheses on the origin of OH/H₂O bearing materials are under
204 consideration: (a) the water and hydroxyl result from chemical reactions between oxides in the
205 lunar soil and protons implanted by the solar wind (*Crider and Vondrak, 2000*), and (b) the water
206 was/is being brought to the Moon by comets, asteroids and meteoroids (*Ong et al., 2010; Bruck*
207 *Syal et al., 2015*). New evidence from LADEE is consistent with meteoritic delivery of water to
208 the Moon (*Benna et al., 2015*). The key question is "what is the role of the solar wind in the
209 formation of the water bearing materials?" Understanding source, accumulation and loss
210 mechanisms for lunar water are of fundamental importance for general planetology as well as the
211 physics and chemistry of surface-space-volatiles interactions.

212 In addition to the local source, there are discussions on the water vapor transport from the
213 equatorial regions to the polar cold traps via the exosphere (*Hodges 1991; Crider and Vondrak,*

SELMA: *How do airless bodies interact with space environment?*

214 2002). The key question is *"how do exospheric gases affect the abundance of water bearing*
215 *materials and vice versa?"*

216 The distribution of hydrogen-bearing materials inferred from the neutron spectrometer
217 measurements differs from the one imaged by M3 in NIR (3 μm) band-depth (linked to OH/H₂O
218 abundance). The signal observed by the neutron spectrometer comes from about the first meter
219 below the surface, whereas the NIR measurement is from the top micrometers of a grain. That
220 implies that the M3 detection of OH/H₂O species is distinctly surface-correlated, i.e., linked to
221 the upper few micrometers of the lunar regolith, but not significantly deeper. The above
222 mentioned infrared studies showed evidence of OH/H₂O at non-permanently shadowed regions,
223 and even at lower latitudes, seemingly more correlated to surface temperature, with daily
224 variations (McCord *et al.*, 2011; Li and Milliken, 2017). This result is controversial since
225 theoretical studies were struggling to explain water accumulated in cold traps over long time-
226 scales, whereas these observations indicated a much more rapid and transient process. While it
227 was pointed out that the infrared observations were highly uncertain at lower latitudes (higher
228 temperature, increasing thermal emission) and could be an instrumental effect (Clark, 2009), the
229 high temporal variability and shallow deposits strongly suggest that solar wind impact plays a key
230 role in water formation on the Moon. FUV observations from LAMP corroborate the diurnal
231 variability of surface hydration (Hendrix *et al.*, 2012). The key question is *"how variable are the*
232 *abundances of the OH/H₂O bearing materials and how is the variability related to the plasma*
233 *and neutral gas environment?"*

234 Because the hydrogen at the lunar surface should be saturated (and result in an equilibrium state
235 between implantation into the grain and loss by diffusion from the grain), the solar wind protons
236 are implanted in several molecular layers into grain surfaces (Load, 1968) or diffuse to the
237 exosphere, escaping to space in a form of atomic neutral H (Hodges, 2011) or molecular
238 hydrogen (Hurley *et al.*, 2017), or being trapped in the permanently shadowed regions as H₂O
239 (Crider and Vondrak, 2000). The balance of hydrogen near the surface has been revealed to be
240 highly controversial against that of laboratory experiments. A high amount of hydrogen is
241 scattered back directly from the lunar surface in contrast to the lab experiments and numerical
242 simulations. Approximately 20% of the solar wind protons are reflected back to space as neutrals
243 with energy > 30 eV (Wieser *et al.*, 2009a; Futaana *et al.*, 2012; Vorburger *et al.*, 2013), 10–
244 50% as H₂ molecules (Hurley *et al.*, 2017) and ~0.1–1% as positively charged ions (Lue *et al.*,
245 2014). Theoretical and numerical interaction models between plasma and lunar regolith, from the
246 solar wind to the final fate, have not yet been established. The key question is *"how does the*
247 *solar wind hydrogen interact with the lunar soil?"*

248 The LCROSS mission investigated the plume caused by the impact of an upper stage rocket into
249 the Cabeus crater close to the lunar South Pole, and observed the water absorption line in the
250 infrared spectrum as well as an ultraviolet emission from hydroxyl radicals, indicating a mass
251 fraction of water in the ejected regolith of 5.6±2.9% (Colaprete *et al.*, 2010). The neutron
252 spectrometer on LRO indicated 0.5–4.0% water ice by weight near the LCROSS impact point
253 (Cabeus), while the water signatures spread to the sunlit region in the vicinity of the crater
254 (Mitrofanov *et al.*, 2010). The Lyman Alpha Mapping Project (LAMP) ultraviolet spectrograph
255 on LRO indicated the presence of about 1–2% water in the permanently shadowed Haworth
256 crater, yet not in the equally shadowed Shoemaker crater, situated just next to it (Gladstone *et al.*,
257 2012). Reported different detections of water ice in different experiments could relate to the
258 depth of the water ice depth. Lunar dusts at the Polar regions could cover the water ice, changing
259 its depth structure. The key question is *"how much is the water buried in the soil of the*
260 *permanently shadowed region and what is its isotope composition?"*

261 **2.1.1 SELMA measurements (water)**

SELMA: How do airless bodies interact with space environment?

262 In order to quantify the solar wind contribution to formation of water bearing materials on the
263 lunar surface, global characterization of the solar wind proton flux at the surface (not at the
264 spacecraft) together with coordinated measurements of the abundance of water bearing materials
265 at surface will be conducted. To differentiate the source of water (solar wind origin or
266 micrometeoroid/cometary origin), a monitoring of dust exosphere (see also Section 2.4) and
267 impact flash measurements is conducted simultaneously. The synthetic, coordinated
268 measurements of in situ and remote sensing measurements are the unique point of SELMA.
269 Isotope composition, in particular for D/H ratio provides direct information on the source of the
270 water at the surface. In addition, thorough measurements at the permanently shadowed regions
271 are conducted to understand if and how the solar wind has direct access to these regions. SELMA
272 undergoes an impact experiment at the end of the mission. An artificial impact into a permanently
273 shadowed region produces a vapor plume and the density and isotope composition of the vapor
274 are made. The information will directly address the source of the water in the cold trap. In
275 addition, the exosphere effects on water bearing minerals are characterized. For this, exospheric
276 gas composition and water-bearing material mapping are correlated. The influences of temporal
277 variations of the environment (both plasma and neutral exosphere) on water bearing-materials are
278 investigated. Long-term correlations between plasma, neutrals, and water-bearing materials at the
279 surface are then taken. Repeated measurements in the Earth's magnetotail (~6 days every one
280 Moon day) help to study the long-term correlation because the solar wind plasma is absent inside
281 the magnetosphere.

282 Overall, these scientific investigations call for the following measurements: Coordinated
283 mappings of the water-bearing minerals (in IR and UV range, like *Pieters et al., 2009* and
284 *Gladstone et al., 2012*) and solar wind flux at the lunar surface (*Futaana et al., 2012*). The spatial
285 resolution of 5 km (typical crater size) for optical (IR and UV) measurements, and that of ~10 km
286 (typical ion gyro radius) for ENA is desired. In addition, environment monitoring is of
287 importance, namely, recordings of upstream solar wind flux (at the spacecraft), the exospheric
288 composition and density, as well as context imaging in the visible range. SELMA further
289 investigates the surface processes and the hydrogen balance by characterizing the scattered
290 hydrogen species in all charge states. Fluxes of H⁺, H⁻, and the neutral H flying from the lunar
291 surface are thus required to be measured. The measurement of the isotope ratios in the exospheric
292 gas and in the impact plume are also a key.

293 These measurements entail the following instrumentations.

- 294 - Spectral imaging in the IR (hydroxyl and water absorption features in the wavelength
295 range 0.4–3.6 μm) and UV (Lyman-α (121.567 nm) and water features (130–190 nm)
296 with spatial resolution <5km.
- 297 - Energetic neutral hydrogen flux in the energy range 10s–a few keV with angular
298 resolution of 5°.
- 299 - Solar wind proton (0.1–10 keV) with 30% accuracy of density and velocity.
- 300 - High mass resolution (M/ΔM > 1000) mass spectroscopy of exospheric gasses to
301 determine the isotope ratio.
- 302 - Visible camera with FoV 60°×30° to monitor the impact flash
- 303 - Dust monitoring to estimate the incoming micrometeoroid flux
- 304 - Hydrogen flux in the energy range a few eV–a few keV for all the charge states separated.

305 In addition, the following instrumentations for the impact experiment are requested.

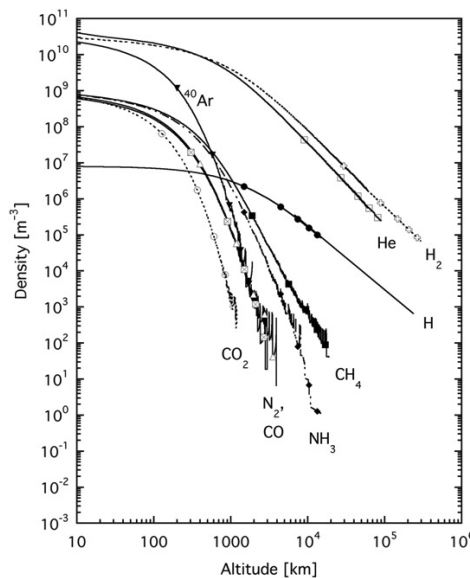
SELMA: How do airless bodies interact with space environment?

- 306 - A mass of 10 kg projectile, with mass spectrometer ($M/\Delta M > 1000$) flying through the
- 307 plume.
- 308 - Context imaging in the visible range during the impact with spatial resolution <100 m.

309 2.2 How do the "volatile cycles" on the Moon work?

310 The lunar exosphere is a key region to understand the water (volatile) cycle at the Moon.
311 Transport of gases within the exosphere is central to the lifecycle of lunar volatiles: it connects
312 the production of volatiles at the surface (by solar wind impact or release by micrometeoroid
313 bombardment), and their sink (photolysis, escape to space or transport to poles). The LADEE,
314 LRO, and ARTEMIS missions have greatly advanced our understanding of the composition and
315 structure of the tenuous lunar exosphere, yet key exospheric constituents such as water and OH
316 remain poorly understood more than forty years after the first Apollo landing.

317 Very low number densities for the lunar exosphere (Figure 2) make the observations difficult.
318 The multiplicity of the mechanisms responsible for the input and loss of species in the exosphere
319 presents modeling challenges. These mechanisms include ion sputtering, photon stimulated
320 desorption (PSD) and micro-meteoroid impact vaporization resulting in inputs to the exosphere,
321 as well as photo-ionization, surface adsorption and escape to space from the lunar gravity field
322 (e.g. Stern, 1999; Wurz et al., 2007, 2012).



323
324 *Figure 2: Density profiles in the lunar exosphere for volatile species on the dayside (at a surface*
325 *temperature of 400K) based on measurements or upper limits (Heiken et al., 1991; Stern, 1999;*
326 *Killen and Ip, 1999). Figure is from Wurz et al. (2012).*

327 Post-Apollo experimental work focused on the neutral sodium (Na) and potassium (K)
328 components of the lunar exosphere, as these can be relatively easily studied from Earth by
329 telescopes (Potter and Morgan, 1988, 1998; Flynn and Mendillo, 1993). The behavior of Na and
330 K is, however, not representative for most of the other species because these two elements are
331 mostly influenced by meteoritic influx and photon-induced desorption (Sprague et al., 1992;
332 Wurz et al., 2007).

333 The composition of noble gases in the lunar exosphere, measured by the Apollo LACE
334 experiment and additionally inferred from studies of gas trapped in lunar regolith samples
335 brought to Earth indicated that species such as helium (He) are dominated by a solar wind source,
336 but with additional contributions probably from the interior of the Moon (Hodges Jr. and

SELMA: How do airless bodies interact with space environment?

337 *Hoffman, 1975; Wieler et al., 1996*). Both LADEE and LAMP observations confirm the solar
338 wind source; they are halted when the Moon is in Earth's magnetotail (*Feldman et al., 2012;*
339 *Cook and Stern, 2014; Hurley et al., 2016; Grava et al., 2016*). Because the solar wind impinges
340 on the lunar surface with energies of about 1 keV / nuc H, He and other solar wind species are
341 absorbed in the surface material (in the regolith grains and rocks) and are trapped. A fraction of
342 the noble gases is subsequently released to become part of the lunar exosphere (e.g., *Hinton and*
343 *Taeusch, 1964; Johnson, 1971; Hodges, 1973*).

344 The flux of heavier, more refractory, elements to the lunar exosphere is dominated by ion
345 sputtering and micrometeoroid impact vaporization (*Wurz et al., 2007*). In this case, the lunar
346 surface material will be the primary source reservoir for elements in the lunar exosphere such as
347 Si, Ti, Al, Fe, Mg, Ca, and O, of which only O has been observed directly (*Cook et al, 2013;*
348 *Vorburger et al., 2014*). However, pickup ions of refractory elements of lunar origin have been
349 identified in the solar wind (*Kirsch et al., 1998; Mall et al., 1998*). Based on modeling (*Wurz et*
350 *al., 2007*), the expected densities of several key elements remain several orders of magnitude
351 lower than present upper limits.

352 Recent measurement by LADEE has identified several neutral species in the exosphere (*Benna et*
353 *al., 2015*), as well as ionized species (*Halekas et al., 2015*). Neutral He contents are controlled by
354 the solar wind alpha particle supply in addition to rather constant endogenous source, i.e.,
355 radioactive decay from the lunar interior (*Benna et al., 2015*). Ne was discovered over the
356 nightside. A localized enhancement of Ar at a specific selenographical region has also been
357 reported (*Benna et al., 2015*).

358 Species detected in the lunar exosphere are the volatile species CH₄ (*Hodges, 2016*), N₂, CO₂, He,
359 NH₃, H₂ (*Stern et al., 2013*), Ne, and Ar. Ionized species, H₂⁺, He⁺, C⁺, O⁺, Na⁺, Al⁺, Si⁺, K⁺, Ar⁺,
360 Ca⁺ and Fe⁺, have also been detected (*Halekas et al., 2013*), providing proof of the existence of
361 the neutral counterpart in the exosphere (*Hartle and Killen, 2006*). Their densities sum up to a
362 total density of about 2·10⁵ cm⁻³ at the surface (*Wurz et al., 2012; Stern, 1999*). In contrast, from
363 the observation of the large electron content in the lunar ionosphere, which is still debated
364 (*Imamura et al., 2010*), one would infer the total neutral density to be at least a factor 10 higher
365 (*Stern et al., 1999*). Alternatively, it has recently been suggested that the dust in the lunar
366 exosphere (*Horányi et al., 2015*) might be the source of these electrons (*Stubbs et al., 2011;*
367 *Szalay and Horányi, 2015*). The lack of measurement in the high-latitude regions during the
368 LADEE mission and the earlier Apollo missions makes it difficult to discuss the localized
369 internal source of neutrals. A global exospheric density mapping will be needed. The SELMA
370 mission will "*fully characterize the lunar exosphere*".

371 The exospheric populations at any moment are given by the strength of the release compared to
372 the loss processes for each species and the population of the species in the lunar exosphere shows
373 temporal variability. The transport cycle in the whole system contributes to the variability.
374 Looking locally, the exospheric composition is determined through balances of atoms and
375 molecules being released from the surface, which can be lost through their escape from the lunar
376 gravity field or transported back to the surface.

377 Some of the release processes are driven by the Sun, i.e., the thermal release (*Stern, 1999*),
378 photon dissociation desorption, and solar wind sputtering (*Hinton and Taeusch, 1964*). These
379 mechanisms will introduce clear daily variations in the lunar exosphere (*Hodges and Johnson,*
380 *1968*). For example, He and Ne follow the exospheric equilibrium for non-condensable gasses
381 with surface temperature (*Benna et al., 2015; Hurley et al., 2016*). The contribution of each
382 mechanism to the source of the exosphere has not been identified. Although the solar conditions
383 (photon flux, heat flux) are rather constant, unique opportunities can happen during lunar eclipses
384 (*Mendillo and Baumgardner, 1995; Potter and Morgan, 1998*). The key question here is "*how is*

SELMA: How do airless bodies interact with space environment?

385 *the lunar exospheric content related to the surface illumination conditions and sources due to*
386 *photon desorption?"*

387 Because of the variable conditions in the solar wind and the existence of the Earth's magnetotail,
388 where the Moon spends 25% of its time near the full moon period, the exosphere has also shorter
389 time-scale variation than a lunar day. Inside the magnetosphere, where no solar wind plasma
390 precipitates, one can expect a change of the plasma production mechanism (Wilson et al., 2006),
391 resulting in a change of the exospheric composition. The exospheric He contents was found to
392 follow the solar wind variation, with an assumption of 4.5-day thermal desorption time constant
393 (Benna et al., 2015). The global characteristics change with the upstream conditions, which
394 address the source and loss mechanisms for the exosphere as a whole, and thus for each species.
395 The key question is "how is the lunar exosphere content related to the plasma environment and
396 sources due to surface sputtering?"

397 Micrometeoroids are another potential source of the lunar exosphere. Such impacts were
398 scientifically first identified only in 1999 as pinpoint flashes (Bellot Rubio et al., 2000). The
399 inflow flux is homogeneous over the surface and will thus add a constant influx of material to the
400 lunar exosphere. Enhancement of the influx during meteor showers will cause a temporal increase
401 in the exosphere of some species (Hunten et al., 1998) as well as the occasional impact of a larger
402 meteoroid on the surface will be observable directly (Mangano et al., 2007). Recently, NMS on
403 board LADEE spacecraft examined the exospheric species changes resulting from Chang'E 3's
404 landing on 14 December, 2013. No large effects on the exosphere by the exhaust materials were
405 detected (Elphic et al., 2014). This could be due to the long time difference and the distance
406 between the measurement place and the landing side (after 30 minutes, LADEE passed the
407 nearest point to the landing site with a separation of 1300 km). In addition, the three primary
408 constituents of the exhaust plume fall in mass channels that have high instrumental background
409 levels. The spatial and temporal variations in the exospheric characteristics are the key to
410 understand its circulation. Therefore, the key question here is "how is the lunar exosphere content
411 related to impact events and sources due to impact vaporization?"

412 The exospheric particles will be lost from the system on specific time scales. Loss mechanisms
413 include surface adsorption or attachment (including those in the cold trap), and escape to space
414 (including direct escape, thermal (Jeans) escape, and via the photo-ionization). Surface
415 attachment is directly associated to the reservoir of volatiles, in particular for the cold traps. The
416 direct escape (when the particles have more speed than the escape speed of 2.4 km/s, on their
417 generation) depends on the source mechanisms. Ion sputtering or scattering may result in direct
418 escape for lighter particles (Thompson, 1968; Wurz et al., 2007), but the photon-stimulated
419 desorption or thermal desorption can hardly produce such high energy particles. The thermal
420 escape might work only for lighter species such like hydrogen or helium (Killen et al., in Press).
421 For most of the heavier particles, the escaping mechanism is via the photo-ionization. The
422 SELMA mission aims to understand "the sinks of the lunar exosphere."

423 2.2.1 SELMA measurements (exosphere)

424 A full characterization of the lunar exosphere will be conducted by the determination of its
425 composition. The composition will be surveyed globally, including the polar regions. Global
426 maps, as well as the altitude profiles of 30–200 km, of the abundances of all main components (H,
427 H₂, He, O, OH, Ne, Na, Ar, K, Ca, CH₄, N₂, CO, CO₂, NH₃, Kr, Xe) are produced. To separate
428 the isotope ratio of the order of 10⁻⁴ between ¹⁶O and ¹⁷O (in the solar system; Yurimoto et al.,
429 2007), M/ΔM>1000 is desired. The investigation of the solar-photon induced exospheric
430 composition will be addressed by measurements of the temporal (daily to monthly) variability of
431 the lunar exospheric compositions. Indeed, a unique opportunity occurs during the lunar eclipses,
432 when the flux of solar photons is completely shut off owing to Earth's shadow. Another temporal

SELMA: How do airless bodies interact with space environment?

433 variation of the exosphere could be induced by the plasma, depending on where the Moon is
434 located (in the solar wind or in the Earth's magnetosphere). To evaluate the plasma contribution
435 to the exospheric content, the correlation between the variations in local plasma conditions and
436 the exospheric characteristics is investigated by coordinated measurements of the plasma and
437 exospheric gas. To quantify the composition of the plasma, separation of K^+ and Ca^+ is aimed
438 (Yokota *et al.*, 2005), corresponding to $M/\Delta M \sim 80$. To investigate impact vaporization as a source
439 of the exospheric material, the correlation between lunar exosphere variations and impact events
440 is explored. Thus, impact events should be measured together with the exospheric gas density.
441 The sink for exospheric species is investigated by measuring escaping particles. The fluxes of the
442 escaping ions (non-thermal) and neutrals (thermal) are quantified to derive the escaping flux from
443 the exosphere to space. Measuring the exospheric ions and neutral species in a wide altitude
444 range is a key measurement for this investigation.

445 These measurements ask for the following key instrument characteristics.

- 446 - Continuous measurements at high mass resolution ($M/\Delta M > 500$) of the composition of
447 exospheric gasses.
- 448 - Ion and electron fluxes in the energy range of 10s eV–a few keV.
- 449 - Ion mass composition ($M/\Delta M > 80$) from the Moon in the energy range of 10 eV–20 keV
450 with moderate (25%) energy resolution
- 451 - Measurements of light flashes from 100 g meteoroids

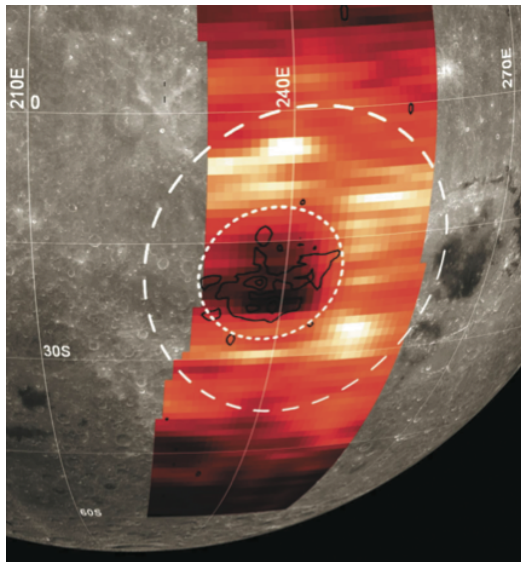
452 **2.3 How do the lunar mini-magnetospheres work?**

453 The Moon currently does not have a global dipolar magnetic field, as would be generated by a
454 liquid metal core dynamo. However, the Moon has localized crustal magnetizations of up to a
455 few 100 nT called magnetic anomalies. These anomalies, first discovered by Apollo 12 (Dyal *et al.*
456 *et al.*, 1970), are spread over the whole surface, mostly clustered on the lunar far side (Richmond
457 and Hood, 2008). They were probably formed early in lunar history when the dynamo was still
458 operating (Purucker *et al.*, 2012). Alternatively, some of the remnant magnetization may be from
459 transient magnetic fields generated during large impact events, through the expansion of an
460 impact-generated plasma cloud in the presence of an ambient magnetic field. This is supported by
461 the apparent location of the largest magnetic anomalies near the antipodes of the giant impact
462 basins (Hood *et al.*, 1991; Wieczorek *et al.*, 2012).

463 The interaction of the magnetic anomalies with the solar wind is of special interest for plasma
464 physics, because it occurs over multiple scales, namely from the fluid scale (plasma can be
465 described as a fluid, on scales larger than the ion scale, >100 km) to the electron scale (electron
466 kinetics are important, <100 m). The effects of magnetic anomalies on the solar wind were
467 detected during the Apollo era as an increase of the solar wind magnetic field caused by the
468 increase of the solar wind density above the anomalies (Russell and Lichtenstein, 1975).
469 Although some numerical studies have been conducted, due to the very small scale (altitude scale
470 is ~ 10 km, which is significantly smaller than the ion scale in the solar wind) and lack of lunar
471 missions for long time after Apollo, no detailed studies had been conducted until 1990s. Electron
472 and magnetic field data from Lunar Prospector over an area of clustered magnetic anomalies at
473 the Imbrium antipode, indicatively showed signatures of a bow shock (Lin *et al.*, 1998) and
474 plasma void (Halekas *et al.*, 2008). It was concluded that a mini-magnetosphere was formed.
475 Such mini-magnetosphere reduces the flux of the solar wind precipitation on the lunar surface as
476 shown in Figure 3 (Wieser *et al.*, 2010; Vorburget *et al.*, 2012; Futaana *et al.*, 2013). The
477 formation, structure and characteristics of the mini-magnetosphere are dominantly controlled by
478 the magnetic field orientation (Deca *et al.*, 2015; Fatemi *et al.*, 2015). In particular, due to the

SELMA: How do airless bodies interact with space environment?

479 lack of the measurement of magnetic field at the surface, we do not know whether the horizontal
480 field plays a more important role than the vertical field (Wang et al., 2013) or vice-versa (Poppe
481 et al., 2016). Overall, the interaction between the magnetic anomaly and the solar wind is highly
482 controlled by the magnetic field geometry. SELMA aims at establishing "the structure and
483 topology of the magnetic field at the surface"



484

485 *Figure 3: Formation of mini-magnetosphere proven by energetic neutral atom measured by*
486 *Chandrayaan-1/SARA instrument. The flux of the emission is proportional to the solar wind flux*
487 *at the lunar surface. The magnetic anomaly influences the solar wind flux close to the surface*
488 *(below the spacecraft). Figure is from Wieser et al. (2010).*

489 Near the magnetic anomaly (and most likely inside the mini-magnetosphere), Lunar Prospector
490 observed increases in low-energy (<100 eV) electron fluxes simultaneously with large magnetic
491 field amplifications, which is consistent with an increase in plasma density across a shock surface.
492 Low frequency wave activity in the magnetic field data (both broadband turbulence and
493 monochromatic waves) was often associated with electron energization, sometimes up to keV
494 energies.

495 Due to the small size of the magnetic anomalies, the mechanism deflecting the solar wind is not
496 well understood (Kallio et al., 2012). Likely, the protons are affected by the ambipolar electric
497 field, which is set-up by the charge separation between magnetized electrons and non-magnetized
498 protons (Saito et al., 2012; Futaana et al., 2013) or by the Hall electric field due to the different
499 motions between the ions and electrons (Järvinen et al., 2014). In addition, at the lunar surface,
500 surface potentials are formed due to the balance between plasma currents and photoelectron
501 currents (Vondrak, 1983). The photoelectron emission from the surface also influence in the
502 electron scale environment near the surface via an electric potential formation (Poppe et al.,
503 2016). In summary, the electrons play significant roles in the interaction region. SELMA
504 establishes "the mechanisms creating small-scale plasma depletions and deceleration of the
505 electrons and ions associated with mini-magnetospheres."

506 Kaguya and Chandrayaan-1 have also conducted in situ measurements of particles and fields
507 above the anomalies. Proton deceleration and electron heating were observed from 100 km down
508 to few 10s km (Saito et al., 2012). The solar wind proton flow deviation above anomalies is
509 detectable up to 100 km altitude and occurs over large areas because the anomalies affect the
510 solar wind in a coherent way (Lue et al., 2011). Over the strongest anomalies up to 50% of the
511 solar wind flux is deflected. This significant flux of the deflected protons causes a change in the

SELMA: How do airless bodies interact with space environment?

512 morphology in the interaction (*Fatemi et al., 2014*) by creating a large-scale disturbance of the
513 solar wind, and trajectories that allow protons to reach the lunar wake and the nightside surface.
514 The key question is "*how does the magnetic anomaly affect the solar wind on the global scale.*"

515 The mini-magnetospheres associated with the anomalies show strong variability with solar wind
516 conditions (*Vorburger et al., 2012*). For example, a mini-magnetosphere associated with an
517 isolated magnetic anomaly close to the Gerasimovich crater shows clear response to the solar
518 wind dynamic pressure. Most other magnetic anomalies (more than half) on the lunar surface
519 have more small-scale features in their magnetic field and do not show such a clear correlation
520 with the solar wind conditions demonstrating a very complex interaction. Lunar Prospector also
521 observed the variability of the anomaly effects on the solar wind depending on the solar wind
522 conditions and solar zenith angle due to the geometrical changes in the solar wind dynamical
523 pressure. Theories and simulations support these observations (e.g. *Fatemi et al., 2015*;
524 *Zimmerman et al., 2015*; *Deca et al., 2015*). The variability of the solar wind flux reaching the
525 surface does affect the proton implantation rate. The key question is "*how do the properties of*
526 *mini-magnetospheres vary with solar wind conditions?*"

527 It was noticed that many of the magnetic anomalies correlate in location with specific albedo
528 features on the surface, called swirls. It was suggested that this is a manifestation of the space
529 weathering effect (*Hood et al., 2001*). Recently, alternative ideas link the differences in albedo
530 with the redistribution of lunar dust, which is charged and thus governed by magnetic and electric
531 fields set up by the interaction between a magnetic anomaly and the solar wind (*Garrick-Bethell*
532 *et al., 2011*). The key investigation is "*the long-term effects of magnetic anomalies on the local*
533 *surface.*" The alternation of the impinging solar wind pattern influences the distribution of the
534 volatiles close to the magnetic anomaly.

535 **2.3.1 SELMA measurements (mini-magnetosphere)**

536 SELMA characterizes the topology of the magnetic field down to the lunar surface. All
537 components of the magnetic field vectors are measured. To establish the small-scale plasma
538 depletion and deceleration mechanisms, ions, electrons and, electromagnetic waves inside the
539 mini-magnetosphere are also measured. The 3-D velocity distributions of ions and electrons (with
540 energy 10s eV–a few keV) are measured simultaneously with the electromagnetic waves to
541 evaluate the dynamics of the environment. These measurements should be conducted very close
542 to the surface down to the electron scale (~100 m). For this investigation, the high time resolution
543 is a key: 0.05 s for fields and 0.5 s for particles. To do this, SELMA is equipped with an impact
544 probe, SIP-MA, which will be released to the Reiner Gamma region.

545 On the other hand, to investigate the global impact of magnetic anomalies on the upstream solar
546 wind characterization of the keV-energy plasma together with knowledge of the local magnetic
547 field is requested. This should be achieved by in situ measurement of 3-D proton and electron
548 velocity distributions and magnetic field. The solar wind impact on the mini- magnetosphere
549 structures can be addressed by energetic neutral atom imaging (*Vorburger et al., 2012*) combined
550 with in situ solar wind monitoring. This measurement requires the ENA imaging with a 10 km
551 resolution because the typical size of the mini-magnetosphere is 100 km. Simultaneously, the
552 solar wind parameters should be obtained. These measurements are conducted by the SELMA
553 orbiter with its altitude coverage of 30–200 km.

554 The study of long-term effects of mini-magnetosphere on the lunar surface, interdisciplinary
555 measurements are coordinated, namely, SELMA combines remote sensing in the wavelength of
556 IR, VIS, and UV ranges together with in situ plasma measurements. Assessment of the lofting
557 dust contribution to the changes in the swirls is also investigated. These interdisciplinary studies
558 are enabled by systematic coordination among the impinging solar wind flux, albedo in the
559 visible range, OH/H₂O related spectra, and local dust measurement (>0.3 μm).

SELMA: How do airless bodies interact with space environment?

- 560 These measurements entail the following key instrument characteristics for the SELMA orbiter.
- 561 - Total ion and electron fluxes in the energy range of 10s eV–a few keV.
 - 562 - Solar wind proton (0.1–10 keV) with 30% accuracy of density and velocity.
 - 563 - Magnetic field vector ranging from 0.1 nT to 5000 nT with an angular accuracy $<10^\circ$.
 - 564 - Energetic neutral atom for the surface imaging with energy of 100 eV–3 keV, with spatial
565 resolution <10 km at the surface.
 - 566 - Visible surface image with resolution <1 km at the surface.
- 567 In addition, the impact probe instrumentations should comply with the followings.
- 568 - Magnetometer >40 Hz with accuracy of $\Delta B < 1$ nT (or $\Delta B/B > 1\%$) for 1–2000 nT.
 - 569 - Ion and electron spectrometer in the energy range of 10 eV–a few keV with a time
570 resolution of 0.5s.
 - 571 - Electric field measurements in the frequency range 1 MHz down to DC.

572 2.4 What is the influence of dust on the lunar environment and surface?

573 The lunar dust environment is expected to be dominated by sub-micron dust particles (*Horányi et al., 2014*). These particles originate from highly weathered lunar regolith. The typical grain size
574 range is from centimeter scale to submicron scale (*Heiken et al., 1991*). During the Apollo era,
575 so-called horizontal glow was unexpectedly discovered by astronauts in orbit. It is caused by
576 scattered sunlight, appearing at the terminators (e.g. *McCoy and Criswell, 1974; Rennilson and*
577 *Criswell, 1974*). This scattered light has been believed to be due to lofted dust, most likely
578 ejected by strong electrostatic forces in the vicinity of the lunar terminator (*Criswell, 1973;*
579 *McCoy and Criswell, 1974; Rennilson and Criswell, 1974; Berg et al., 1976; Zook and McCoy,*
580 *1991*). Modeling efforts suggested a significant dust exosphere (typical grain size of 0.1 μm) over
581 the terminator region, extending to altitudes above 100 km, with an integrated column density of
582 10^{-10} kg/m². (*McCoy 1976; Zook and McCoy 1991; Murphy and Vondrak, 1993*). The
583 electrostatic forces that make the dust grains lofted have been discussed (*Stubbs et al., 2006* and
584 reference there in), but no firm conclusion has been provided. Recent fully kinetic calculations
585 show the effect of electric fields on the lunar dust populations (*Dyadechkin et al., 2015; Kallio et al., 2016*).
586 One of the main difficulties in the discussions about the dust environment is the lack
587 of the in situ measurements of dust grains.
588

589 The first attempt to observe the lunar ejecta cloud by the Munich Dust Counter on board the
590 HITEN satellite orbiting the Moon (15 February 1992 to 10 April 1993) did not succeed, owing
591 to its distant orbit and low sensitivity (*Iglseder et al., 1996*). The Lunar Dust Experiment (LDEX)
592 onboard NASA's Lunar Atmosphere and Dust Environment Explorer (LADEE) began its
593 measurements on 16 October 2013 and detected a total of approximately 140,000 dust hits in the
594 altitude range of 1-250 km during about 80 days of cumulative observation time out of 184 total
595 days by the end of the mission on 18 April 2014 (*Elphic et al., 2014*). LDEX was designed to
596 explore the ejecta cloud generated by sporadic interplanetary dust impacts, including possible
597 intermittent density enhancements during meteoroid showers, and to search for the putative
598 regions with high densities of 0.1- μm -scale dust particles above the terminators (*Horányi et al.,*
599 *2014*). Due to the limitation of the orbiter trajectory, only the equatorial region ($\pm 22^\circ$ from the
600 lunar equator) was explored. Therefore, SELMA will complete the emerging picture, "fully
601 characterizing the missing portions of the lunar dust environment."

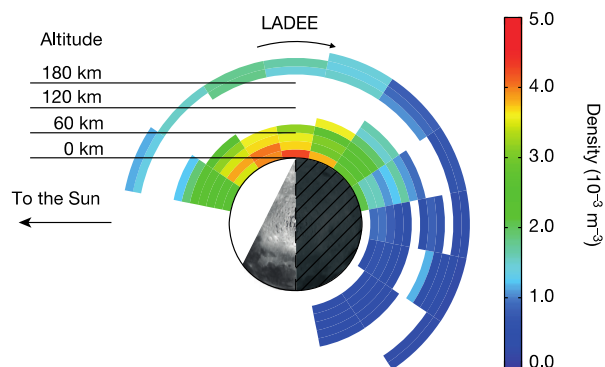
602 There are two main mechanisms for maintaining the lunar dust cloud: 1. ejecta production by
603 continuous bombardment of interplanetary dust particles; and 2. the putative electrostatic lofting

SELMA: How do airless bodies interact with space environment?

604 of surface materials. The Moon is continually bombarded by interplanetary dust, liberating orders
605 of magnitude more solid ejecta than the impacting particles. Only a small fraction of the impact
606 generated ejecta particles escape lunar gravity, and most of them follow ballistic orbits and form
607 a gravitationally bound dust exosphere around the Moon. IDPs are delivered to the Moon at a rate
608 of ~ 5000 kg/day (Grün et al. 1985). Their characteristic radius is ~ 100 μm with typical speeds of
609 20 km/s (Taylor 1996). Those ejected particles form the dust cloud (Grün et al., 2011). The lunar
610 dust cloud was first observed by LDEX (Horányi et al., 2015; Figure 4). Ejecta clouds were also
611 observed by the Galileo mission during flybys of the icy moons of Jupiter: Europa, Ganymede
612 and Callisto (Krueger et al., 2000).

613

614



615

616 *Figure 4: The top-down view of the dust particle density ($a > 0.3 \mu\text{m}$) projected onto the lunar*
617 *equatorial plane. While pointed near the direction of the motion of the spacecraft, LDEX did not*
618 *make measurements between 12 and 18 local time. White coloring indicates regions where*
619 *LADEE did not visit or was not set up for normal operations. Figure is from Horányi et al.*
620 *(2015).*

621

622 Strong temporal variability of the dust density was observed by LDEX on LADEE, most likely
623 associated with the stochastic nature of the meteoroid impacts. Moreover, intermittent density
624 enhancements were also observed during several of the annual meteoroid streams (Horányi et al.,
625 2015). Clear spikes in the dust impact rate during the well-known meteor shower (for example by
626 Taurids and Geminids) were detected. On the other hand, the rendezvous of LADEE with
627 Chang'E-3 landing (Elphic et al., 2014) did not provide any clues of dust signals. It is very
628 unlikely to be observed because the separation between the two spacecraft was too large.

629 Nevertheless, LDEX measurements during intense meteoroid showers indicated strong
630 correlations with dust influx. However, the quantitative assessment between the dust cloud and
631 the impact flux could not be fully characterized based on LDEX measurements alone. In addition,
632 the question of what is the direct influence by a relatively large impact to the dust cloud still
633 remains. The key question is "how do the impact events affect the lunar dust environment?"

634 Another putative source mechanism for high altitude lunar dust is electrostatic lofting. UV
635 radiation and/or solar wind plasma near the surface is expected to induce intense electric fields
636 near the terminator region (Sternovsky et al., 2008). The electric field may loft dust particles with
637 characteristic radii of $\sim 0.1 \mu\text{m}$ (McCoy and Criswell 1974; McCoy 1976). This phenomenon is
638 preferably occurring near the terminator region, where the sunlit and shadow boundary exists.
639 The effect of varying surface potentials because of shadowing on the lofting of lunar dust was
640 shown in recent simulations (Dyadeschkin et al., 2015). Due to the different illumination

SELMA: How do airless bodies interact with space environment?

641 conditions, the surface potentials may differ (Vondrak, 1983), and strong electric fields are
642 expected to exist. Due to the coincidence of the strong electric field potentials and the scattered
643 sunlight measured by Apollo astronauts, the lofted dust particles are assumed to be responsible
644 for the horizontal glow.

645 However, the processes involved remain controversial. Observations by the star tracker camera
646 onboard the Clementine (Glenar et al., 2014) and the LAMP instrument onboard the LRO
647 (Feldman et al. 2014) indicate the upper limits for the density of the high altitude dust exosphere
648 lower than the previously reported densities. LDEX did not find any evidence for the expected
649 density enhancements over the terminators (Horányi et al., 2015). Overall, no observations (other
650 than the indirect evidence of horizontal glow) have successfully supported the existence of lofted
651 dust. As of yet, unknown conditions or UV illumination and/or plasma exposure may be
652 important to generate electrostatic dust lofting. The key question is "how might plasma effects
653 result in lofting the lunar dust?"

654 **2.4.1 SELMA measurements (dust)**

655 SELMA will be the first to fully characterize the global lunar dust environment. Correlations
656 between the variability of the global dust distribution and the exospheric profiles will be taken;
657 the investigation is realized by simultaneous time-series measurements of dust characteristics and
658 the exospheric composition and spatial profile. As the lunar dust environment is thought to be
659 dominated by submicron-sized dust, the dust size distribution down to 0.3 μm is measured. To
660 understand the origin of the lunar dust environment, correlations between impact events (both
661 natural bombardment of >100 g meteoroid or artificial impactor) and dust profiles are to be
662 investigated. Simultaneous measurements of the dust size distribution and monitoring of the
663 meteoroid impact are necessary. An artificial impactor of 10 kg would realize the measurement.
664 The correlation of the dust population with the plasma environment will also be investigated. It is
665 realized by characterizing the dust environment while simultaneously monitoring the plasma
666 particle populations and electric and magnetic fields. Simultaneous measurements of the dust size
667 distribution and plasmas observations are thus conducted.

668 These measurements call for the following key instrument characteristics for the SELMA orbiter.

- 669 - Dust flux $>0.3 \mu\text{m}$ ($>10^{16}$ g)
- 670 - Electric field from DC–1 MHz
- 671 - Continuous measurement of high mass resolution ($M/\Delta M > 500$) mass spectroscopy of
672 exospheric gasses.
- 673 - Measurements of light flashes from 100 g meteoroids

674 In addition, the following instrumentations for the impact experiment are requested.

- 675 - A mass of 10 kg projectile into a known permanently shadowed crater.
- 676 - Electron 3D distribution functions with time resolution of 0.5 s
- 677 - Electric and magnetic field

678 **3 SELMA mission**

679 **3.1 SELMA mission overview**

680 The SELMA mission is designed to achieve the SELMA science objectives (Table 1). For this
681 purpose, the SELMA mission includes an orbiter, an impact probe SIP-MA, a passive impactor,
682 and a simple relay CubeSat (RCS) (Table 2). The SELMA orbiter is inserted into a low

SELMA: How do airless bodies interact with space environment?

683 maintenance quasi-frozen orbit 30×200 km with the pericenter over the South Pole, similar to the
684 NASA Lunar Reconnaissance Orbiter (LRO) orbit. The lifetime is 15 months in order to cover all
685 the known meteor shower events. All instruments operate throughout the whole missions.

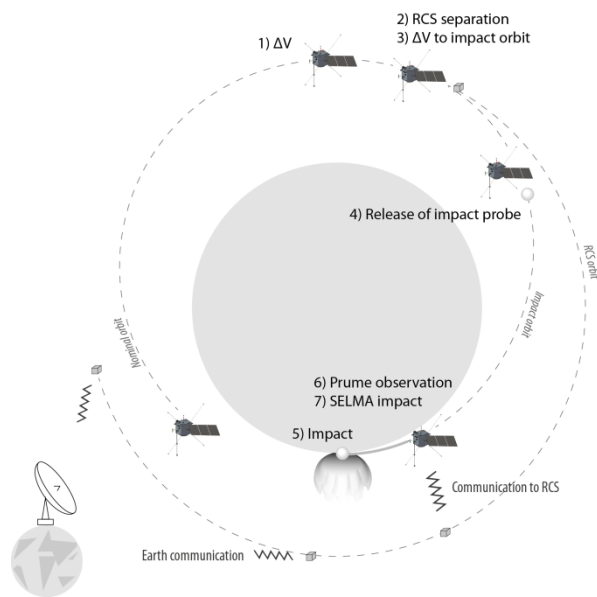
686 *Table 2: SELMA mission elements and their time line and the lifetime*

Elements	Time line	Life time
SELMA orbiter	Moon orbit insertion after 4–5 days after launch	15 months
SIP-MA	Impact probe experiment 6 months after launch	30 min.
Impactor (passive)	Impact experiment 15 months after launch	30 min
RCS	Impact experiment 15 months after launch	87 min

687 Two impact experiments are conducted during the mission. The first impact experiment is at six
688 months after the launch; the impact probe SIP-MA is released targeting the Reiner-Gamma
689 magnetic anomaly region to address the "mini-magnetosphere" science. During the descent SIP-
690 MA transmits the data to the SELMA orbiter. The lifetime of SIP-MA is ~30 min. The
691 requirement is that the experiment is done when the Moon is in the solar wind, and when the
692 solar zenith angle of the target magnetic anomaly is 40–60°. The primary target is the Reiner
693 Gamma area (*Hood et al., 1979*). This required geometric constellation is realized every month.
694 Therefore, there are no requirements of the experiment time. Here tentatively we assumed to
695 conduct the measurement 6 months after the SELMA launch.

696 The second impact experiment is for the direct measurement of the water content inside the
697 permanently shadowed region (for "water" science, as well as "exosphere" and "dust" sciences).
698 This is conducted at the end of the mission. The target is, as a primary candidate, the Shackleton
699 crater. The sequence is summarized in Figure 5. Two elements are released: a passive impactor
700 and a relay cubesat (RCS). The passive impactor targets the permanent shadowed region to make
701 an artificial impact. Prior to the impact, the SELMA orbit is changed to a circular lunar orbit
702 (CLO) of 400 km altitude (1) to increase the impact angle to 10°. After a few orbits, RCS, serving
703 as a data relaying satellite during the SELMA impact, is released with a low ΔV (2). RCS closely
704 follows SELMA in its CLO. Shortly after the RCS release, SELMA performs a ΔV -maneuver
705 targeting a point of impact in the Shackleton crater (3). Immediately after the impact maneuver, a
706 passive impactor is separated (4) to impact the surface >10 sec ahead of SELMA to create a
707 plume (5), which the SELMA orbiter investigates before the impact (6). The SELMA orbiter will
708 crash to the surface in the end (7). During the descent the science data are continuously
709 transmitted from SELMA the ground and to the RCS, still in its 400 km altitude orbit, that stores
710 the data on-board for later downlink to Earth. RCS is required to record the data when SELMA is
711 in the crater out of visibility from the ground and to back-up the data received during this critical
712 operation.

SELMA: How do airless bodies interact with space environment?



713

714 *Figure 5: Impact experiment sequence to investigate a permanently shadowed region (not in*
715 *scale).*

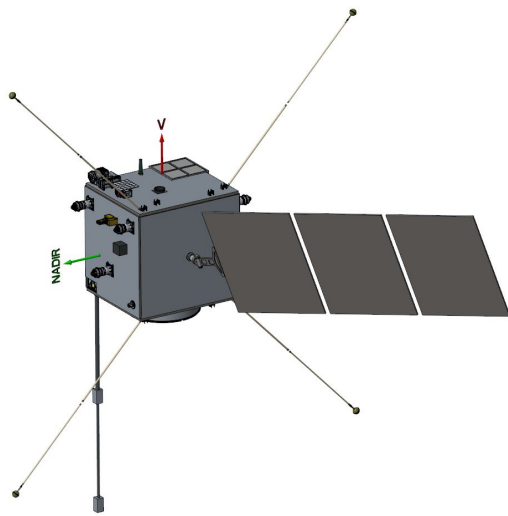
716 3.2 SELMA mission elements

717 3.2.1 SELMA orbiter

718 The SELMA orbiter is designed to accomplish a majority of the scientific objectives. The orbit of
719 30–200 km is the primary requirement; the pericenter altitude was defined from the precise
720 imaging for "water" science as well as the in situ measurements needed for the "mini-
721 magnetosphere" science. The pericenter latitude is at the South Pole, because of the concentrated
722 permanently shadowed region at the South Pole, as well as the aggregation of the magnetic
723 anomalies in the southern hemisphere. The apocenter altitude was defined to enable monitoring
724 of the global meteoroid impacts (influencing "volatile cycles" and "dust" sciences) and to meet
725 the need for altitude profiles of the exospheric composition (for "volatile" sciences). The mission
726 length is for 15 months, which cover one full Earth year observation so that the mission covers all
727 meteor shower events, maximizing the opportunity of detecting impact events. The launch date is
728 flexible.

729 The SELMA orbiter is a 3-axis stabilized spacecraft. The SELMA orbiter hosts four remote-
730 sensing instruments and seven in situ instruments. These sensors are accommodated to conduct
731 the coordinated observations; for example, the co-aligned remote-sensing sensor fields of view.
732 All the sensors are operated continuously. Figure 6 shows the SELMA orbiter design. Four
733 booms are deployed for the electric field measurements, and a single boom for the magnetic field
734 measurements.

SELMA: How do airless bodies interact with space environment?

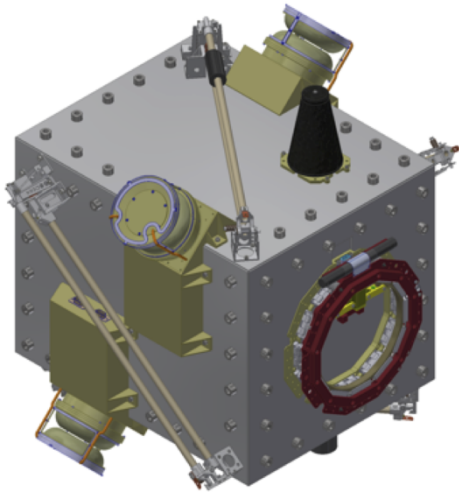


735

736 *Figure 6: SELMA orbiter design. The SELMA orbiter is a 3-axis stabilized platform, with a solar*
737 *array with a 2-axis driving mechanism on one side of the bus in order to realize continuous*
738 *measurements over the one Earth year (mission lifetime). The remote sensing instruments are*
739 *mounted in the nadir deck (green arrow in the figure), always pointing to the lunar surface,*
740 *sharing the same boresight. In situ instruments are located either the nadir deck, ram deck (red*
741 *in the figure), or zenith deck (anti-nadir direction, not visible in the figure). Four long booms are*
742 *for the electric field measurement (Orchestra), and another boom is for magnetometer. The*
743 *block at the top-right corner is the SIP-MA (See section 3.2.2).*

744 **3.2.2 SELMA Impact Probe-Magnetic Anomaly**

745 Some of the scientific objectives for the "mini-magnetosphere" science require the very low
746 altitude measurement (0.1 km altitude) inside a magnetic anomaly. A dedicated impact probe is
747 thus launched from the orbiter. The impact probe, SELMA Impact Probe-Magnetic Anomaly
748 (SIP-MA), flies through the mini-magnetosphere to measure the plasma characteristics using very
749 high-time resolution instruments. After the measurement, SIP-MA will crash into the lunar
750 surface. The key region is below an electron gyroradius (0.1 km; 10 eV electron under 100 nT).
751 Figure 7 shows the SIP-MA mechanical design. Four booms for field measurements are deployed
752 after the separation. The measurements are conducted down to the altitude range below 0.1 km.
753 To descent from the altitude of 0.1 km to the surface to crash, SIP-MA typically takes 1–3 s
754 (assuming 1–2° of impact angle). Thus, 3-D proton and electron distribution with full angular
755 coverage within 0.5 s, together with DC electromagnetic fields are measured. Four in situ sensors
756 are accommodated (see Section 4 for details).



757

758 *Figure 7: SIP-MA mechanical design. Red-colored ring structure in the right is the separation*
759 *ring. Four sensor heads (three are visible in this figure) are for the ion and electron*
760 *spectrometers to cover 4π field of view together, and the four booms (two are visible) are*
761 *deployed for electric (mini-EF) and magnetic (IPMAG) fields.*

762 **3.2.3 Passive impactor:**

763 To produce the enough material from the permanently shadowed crater for the impact experiment,
764 a passive impactor is prepared. It is a 10 kg copper sphere, with which Holsapple and Housen
765 scaling law model (<http://keith.aa.washington.edu/craterdata/scaling/index.htm>; *Housen and*
766 *Holsapple, 2011*) predicts ~ 700 kg ejecta. Assuming 6% water content in the permanently
767 shadowed crater (*Mitrofanov et al., 2010*), 40 kg (2000 mol) of water molecules are released.
768 Assuming a 10 km scale plume ($\sim 10^{18}$ cm³), the density becomes of the order of 10^9 cm⁻³. While
769 the water molecule content in the regolith is highly uncertain, and the assumed 6% is the highest
770 value ever reported: a 10 kg impactor produces 10^3 – 10^4 times higher density of water compared
771 to the natural exosphere (10^5 – 10^6 cm⁻³). To have sufficient sampling time for the mass
772 spectrometer inside the plume, the spacecraft has to travel through the plume for longer than 10 s.

773 **3.2.4 Relay CubeSat**

774 A relaying cubesat, RCS, is released in order to receive the measured data by the SELMA
775 orbiter during the last seconds. The received data will be transferred to Earth. RCS is required
776 because the SELMA orbiter becomes invisible from Earth when it enters to the shadowed crater.
777 RCS is a 6U cubesat, with S-band communication package and a simple camera to monitor the
778 SELMA impact.

779 **4 Science payload**

780 Table 3 summarizes the proposed science payload and their key measurements, as well as the
781 required key performance to satisfy the SELMA science cases. Tables 4-6 show the summary of
782 payload performance.

783

784 *Table 3: SELMA science payload and the required key performance. Contributions to the science*
785 *questions are also indicated by X (for major contribution) and x (for interdisciplinary*
786 *contribution)*

Instrument name	Full name	Key measurement	Key performance	Water	Exosphere	Mini-magnetos	Dust
SELMA orbiter							
VIS-NIR	IR and visible spectrometer	H ₂ O/OH/ice detection on the surface	Spectral range 400 – 3600 nm	X		X	
SPOSH	Wide angle and transient phenomena camera	Surface context imaging, transient phenomenon detection, meteoroid impact	Visible range; FoV: 120°x60° Meteoroid mass: 10s g- 1 kg	X	X	X	X
MUVS	Moon UV imaging spectrograph	Surface UV spectroscopy	Spectral range 115–315 nm	X	X	X	
ENAT	ENA telescope	Backscattered hydrogen to monitor proton flux impinging the surface	Energy range 10 eV–3 keV. Ang. resol. < 10°	X	X	X	
LIS-SW	Lunar positive ion spectrometer	Positive SW ion distribution functions	Energy range 1 eV–10 keV 3D coverage (2π)	X	X	X	(x)
LIS-MS	Positive ion mass spectrometer	Positive ion mass composition Secondary ion mass spectroscopy	Energy range 10 eV–1 keV 3D coverage (2π) M/q > 2 M/ΔM > 50	(x)	X	X	(x)
LSHE	Lunar scattered proton and negative ions experiment	Scattered negative hydrogen and proton distribution functions Solar wind monitoring from nadir plane	Energy range 1 eV–10 keV 3D coverage (2π)	X	X	X	(x)
LES	Lunar electron spectrometer	Electron distribution functions	Energy range 1 eV–10 keV 3-D coverage (4π) Time resolution 1 sec		X	X	X
MMAG	Moon Magnetometer	Magnetic field vector	0.1–30000 nT ΔB < 0.1 nT			X	X

SELMA: How do airless bodies interact with space environment?

	ter					
LEMS	Lunar Exospheric Mass Spectrometer	Exosphere composition and content	$M/\Delta M > 1000$	X	X	X
Orchestra	Plasma Wave Instrument	Plasma waves and electric field	Sampling frequency 10 kHz $\Delta E < 1\text{mV} / \text{m}$	X		X
LDD	Lunar Dust Detector	Dust size, fluxes, and velocities	Dust particle mass down to 10^{-16} kg			X
SIP-MA						
MiniEF	Waves and electric field	Electric field measurement	Frequency 1.4 MHz Spatial resolution 100 m			X X
IPEI	Impact probe ions and electrons spectrometer	Ion and electron distribution functions	Energy range: a few eV–a few keV Time resolution: 0.5s/3D 3D coverage (4π)			X
IPMAG	Impact probe magnetometer	Magnetic field vector	Range: 0.1 – 30000 nT $\Delta B < 0.1$ nT			X
IPCAM	Context camera	Context imaging PR imaging	Video stream			X
Impact experiment						
Passive impactor (*)		Passive impactor	10 kg	X	X	X
IECAM	Context camera	Context imaging PR imaging	Video stream	X		

788
789
790
791

792 *Table 4: SELMA orbiter remote sensing instrument performances*

793

Instrument	VIS-NIR	SPOSH	MUVS	ENAT
Objective	Photon	Photon	Photon	ENA
Spectral range	400–3600 nm	400–800 nm	115–315 nm	
Spectral	$\lambda/d\lambda = 100$		1.2 nm	

SELMA: How do airless bodies interact with space environment?

resolution				
Field of view	3.2°	61.7°	0.3x7.5°	10x10°
Angular resolution	0.015°	0.031°	0.06°	5x5°
Sampling time	<6 ms			0.5s
Energy range				10 eV–3 keV
Energy resolution				50%
Mass range				1–70 amu
Mass resolution				H and heavies

794

795 *Table 5: SELMA orbiter and SIP-MA in situ particle instrument performances*

Instrument	LIS-SW	LIS-MS	LSHE	LES	LEMS	LDD	IPEI
Target	Positive ions	Positive ions (M>=2)	H ⁺ , H ⁻	Electrons	Neutral	Dust	H ⁺ , e ⁻
Energy speed range	1 eV–10 keV	1 eV–1 keV	25 eV–40 keV	<15 keV	0–10 eV	> 1km/s	< 15keV
Energy resolution	15%	25%	7%	10%	N/A		10%
FOV	360°x90° (2π)	360°x90° (2π)	360°x90° (2π)	4π	360°x10°		4π for each
Angular resolution	22.5x11.25°	22.5x11.25°	22.5x5°	22.5x5°	N/A		22.5x5°
Sensitivity, G-factor	10 ⁻³ cm ² sr eV/eV	Flux of 10 ⁴ /cm ² s	10 ⁻² cm ² sr		1 / cm ³ s		
Time resolution	2s	3s		0.5s	1–100s	0.1s	0.5s
Mass range		2–150 amu			1–1000 amu		N/A
Mass resolution		>80			1100		N/A
Impact charge range						3x10 ³ –10 ⁷ e-	
Impact charge uncertainty						10%	
Cumulative charge deposition rate						5x10 ⁴ e/s	

796

797 *Table 6: SELMA orbiter and SIP-MA field sensor performance*

Instrument	MMAG	Orchestra	IPMAG	Mini-EF
Platform	Orbiter	Orbiter	SIP-MA	SIP-MA
Target	Magnetic field	Electric field	Magnetic field	Electric field

Range	±64000 nT	DC–1.4 MHz	±10000 nT	DC–1.4MHz
Resolution	8 pT			
Sensitivity	< 10 pT/√Hz		< 20 pT/√Hz	
Electron density		10-4–10 ⁵ cm-3		
Electron temperature		0.01–100 eV		

798

799 **4.1 IR and visible spectrometer (VIS-NIR)**

800 The IR spectrometer for SELMA is based on the heritage of the SIR-2 spectrometer (*Mall et al.,*
 801 *2009*) and the experience of the M3 instrument on Chandrayaan-1 (*Pieters et al., 2009*). The
 802 spectrometer consists of an optical unit, a wedge filter (or Linear Variable Filter, LVF), a dual-
 803 hybrid detector and a thermoelectric cooler. A LVF is a band-pass filter whose coating has been
 804 intentionally wedged in one direction. Since the band-pass' center wavelength is a function of the
 805 coating thickness, the peak wavelength transmitted through the filter will vary in a linear fashion
 806 in the direction of the wedge. The LVF has at a given point a Gaussian transmission profile, at
 807 which radiation is transmitted. The LVF has a range between 0.4 to 3.6 μm over a length of
 808 approximately 10 mm. The filter is mounted on a substrate, which exactly fits the detector. The
 809 dual-hybrid detector (silicon for pixels 1–70 and HgCdTe for pixels 71–280) is thermally
 810 insulated and is cooled and stabilized through a four-stage Peltier element. The option with a
 811 radiator similar to the Chandrayaan-1/SIR-2 is also available and used for the spacecraft
 812 mechanical layout. The spectral dispersion is achieved only through the LVF. The optics have a
 813 focal length of 150 mm and an f-number of 4.5 yielding an IFOV of 0.015° per pixel which
 814 corresponds to a ground-sampling distance of 20 m/pixel at an altitude of 100 km. At a spin rate
 815 of 1 rpm, the resulting dwell time for one IFOV will be around 6 ms. The active FOV is
 816 3.2°×3.2°.

817 **4.2 Wide angle and transient phenomena camera (SPOSH)**

818 The SELMA wide-angle camera, based on the Smart Panoramic Sensor Head (SPOSH), is a
 819 frame camera built to observe meteoroid impacts and possible other luminous night time
 820 phenomena in the visible range (400–800 nm) on the dark hemisphere of the Moon (*Oberst et al.*
 821 *2011*), and will allow detection of any meteoroid impact with a mass larger than a few grams. In
 822 spite of the highly sensitive CCD (1024×1024 pixels), we foresee limited daylight operation for
 823 context imaging. The camera contains a camera head that consists of an optical telescope with a
 824 wide-angle lens and a detector unit. The highly sensitive CCD allows the detection of impact
 825 flashes on the dark side of the Moon. The digital processing unit (DPU) uses powerful event-
 826 detection software, and in impact flash search operations the DPU will reduce the data stream
 827 dramatically by transmitting only those portions of images that contain events.

828 **4.3 Moon UV imaging Spectrograph (MUVS)**

829 MUVS is a long-slit ultraviolet imaging spectrograph, with a spectral bandpass including far- and
 830 mid-ultraviolet wavelengths in the 115–315 nm range, which will be used to: 1) Measure the
 831 surface water frost abundance in permanently shadowed regions; 2) Characterize the diurnal
 832 transport of water/hydration across the lunar surface; 3) Identify space weathering processes by
 833 surveying lunar swirl features; and 4) Investigate the exospheric response to SELMA's impact
 834 probes and also natural meteor streams. MUVS builds upon the legacy of LAMP's UV spectral
 835 mapping (*Gladstone et al., 2010*) with the improved sensitivity, spatial resolution, and spectral
 836 coverage. By extending the wavelength to 315 nm compared to LRO/UVS), we will search for

SELMA: How do airless bodies interact with space environment?

837 OH (308 nm) in the exosphere, as well as other components (Mg at 285 nm, Fe at 272 nm, and Si
838 at 252 nm).

839 The MUVS telescope feeds a 15-cm Rowland circle spectrograph with a spectral bandpass of
840 115–315 nm. The telescope has an input aperture 4×4 cm² and uses an off-axis parabolic (OAP)
841 primary mirror. Light from the OAP is focused onto the spectrograph entrance slit, which has
842 field-of-view of 0.3°×7.5°. Light entering the slit is dispersed by a toroidal diffraction grating that
843 focuses the UV bandpass onto a curved microchannel plate (MCP) cross strip (XS) detector. The
844 MCP uses atomic layer deposition (ALD) coated borosilicate glass plates with a solar blind, UV-
845 sensitive GaN photocathode applied to enable mid-UV sensitivity; a sealed tube vacuum and
846 MgF₂ window are used to keep this photocathode pristine, post-assembly.

847 **4.4 ENA Telescope (ENAT)**

848 The ENA telescope (ENAT) is based on the CENA (Chandrayaan-1 Energetic Neutrals Analyzer)
849 and ENA (Energetic Neutrals Analyzer) instruments for the Chandrayaan-1 and BepiColombo
850 missions (*Barabash et al., 2009; Saito et al., 2010*). ENAT has a factor-of-10 better angular
851 resolution and a factor-of-10 larger geometrical factor than them. Signal processing is a heritage
852 from the SWIM (Solar Wind Monitor) sensor on Chandrayaan-1 (*Barabash et al. 2009*).

853 ENAT consists of four building blocks, a charged particle deflection and collimator system, a
854 surface ionization section, an energy analyzer and a time-of-flight section. The charged particle
855 deflection and collimator section rejects charged particles up to 10s keV by electrostatic
856 deflection. As opposed to its predecessors, ENAT features only one single viewing pixel with
857 5°×5° angular pixel size, but with a much larger geometric factor. The generated positive ions are
858 extracted from the conversion surface, energy analyzed in a wave shaped energy analyzer and
859 post-accelerated by 2.4 kV. Ions are then guided to the time-of-flight section of the instrument
860 where they hit a highly polished tungsten single crystal surface. The interaction with the surface
861 generates a secondary electron that is measured using a channel electron multiplier (CEM),
862 providing the start signal for the time-of-flight measurement. The ion is most likely neutralized in
863 the process and travels to the stop surface located a short distance away where another secondary
864 electron is generated. This electron is collected by another CEM providing the stop signal of the
865 time-of-flight measurement. The combination of time-of-flight section and the energy of the
866 particle allow us to calculate the mass of the particle.

867 **4.5 Lunar positive ion spectrometer (LIS)**

868 The Lunar positive ion spectrometer (LIS) consists of two sensors: a) the Ion Spectrometer for
869 Solar Wind (LIS-SW) and b) Ion Spectrometer for Mass Spectrometry (LIS-MS). The
870 Cluster/CIS/HIA and CODIF, Cassini/CAPS, BepiColombo/MEA and MSA, Solar
871 Orbiter/SWA/PAS, and JUICE/PEP/JDC sensors provide significant heritage for LIS.

872 The LIS-SW sensor consists of one compact, low mass, highly capable sensor based on a design
873 carefully and specifically optimized for the ion bulk properties (density, velocity and
874 temperature) of the solar wind. The sensors providing fast 3-D measurements in the energy range
875 1 eV–10 keV are customized for the energy range as well as the dynamic range encompassing
876 solar wind as well as magnetospheric suprathermal and thermal plasma originating from the Earth
877 when the Moon is embedded within the terrestrial magnetosphere. The LIS-SW sensor consists of
878 five main structural elements: 1) the electrostatic entrance deflector selects incident positively
879 charged particles entering at elevation angle and steers them into the electrostatic analyzer; 2) the
880 electrostatic analyzer selects the energy passband by setting voltages on an inner plate; 3) the
881 detector board includes 16 ceramic CEM along the periphery; 4) the HVPS and FPGA boards

SELMA: How do airless bodies interact with space environment?

882 situated below the detector plane; 5) an electronic box containing LVPS and DPU boards
883 common to both LIS-SW and LIS-MS contains the rest of the subsystems.

884 LIS-MS sensor will provide lunar surface and exospheric composition information through
885 secondary ion mass spectrometry. It will measure the secondary ions sputtered from the regolith
886 grains by solar wind ion bombardment. The LIS-MS resolves lunar secondary ion fluxes ranging
887 between ~ 10 and 10^4 ions $\text{cm}^{-2} \text{s}^{-1}$ (depending on the species) but excluding high solar wind
888 proton flux and photon background.

889 The LIS-MS sensor consists of five main structural elements: 1) the electrostatic entrance
890 deflector selects incident positively charged particles entering at elevation angle θ and steers them
891 into the filtering chamber; 2) the filtering chamber which should prevent the proton and photon
892 background to enter contaminate the reflectron chamber and let the minor and trace species
893 access the reflectron chamber; 3) the reflection time-of-flight chamber where the selection of ions
894 with m/q is achieved; 4) the HVPS and FPGA boards attached to the sensor head; 5) the
895 electronic box containing LVPS and DPU boards is common to both LIS-SW and LIS-MS.

896 **4.6 Lunar scattered proton and negative ions experiment (LSHE)**

897 LSHE observes and measure the distributions of scattered negative hydrogen, protons and alpha
898 particles in the energy range from 25 eV to 40 keV. The LSHE instrument is based on the design
899 of IMA/MEX, IMA/VEX and ICA on Rosetta. It comprises a top-hat design (16 sectors over
900 360° entrance) and uses a magnetic mass separation system. Ions entering LSHE first pass
901 through a semi-spherical electrostatic energy analyzer, then a two-slit electrostatic lens, and
902 finally the mass analyzer where a cylindrical magnetic field created by permanent magnets
903 separates the trajectories of different ion species, according to their mass per charge. The particles
904 are detected by an MCP which comprises an anode system with 32 rings representing ion mass.

905 **4.7 Lunar Electron Spectrometer (LES)**

906 The LES instrument will determine the electron density, temperature and the velocity distribution
907 functions of the local plasma environment of the spacecraft. The baseline design will address this
908 with two top-hat type electrostatic analysers, each with a FoV deflector system to allow
909 electrostatic deflection of incoming electrons by up to $\pm 45^\circ$ out of the plane of the undeflected
910 FoV. The two sensors will be accommodated on the nadir and zenith faces, close to the edges or
911 corners of the spacecraft.

912 Incoming charged particles enter the sensor through the exterior electrically grounded aperture
913 grid. The particles are steered from the arrival direction into the hemispheric Energy Analysis
914 section using voltages applied to either the upper or lower deflector electrodes providing a Field-
915 of-view Deflection System. The EA section permits only electrons of the selected energy and
916 type to reach the detector subsystem consisting of a micro-channel plate (MCP) detector.

917 **4.8 Moon Magnetometer (MMAG)**

918 The MMAG instrument measures the magnetic field in the vicinity of the spacecraft. This is
919 crucial for characterizing lunar magnetic anomalies and revealing how they interact with the
920 ambient collisionless plasma environment (solar wind as well as the Earth's magnetosheath and
921 magnetotail). Previous implementations of the fluxgate sensors and associated electronics have
922 flown on missions such as Cassini and Double Star, and are included in the planned Solar Orbiter
923 and JUICE magnetic field investigations, providing highly relevant, direct heritage (*Dougherty et*
924 *al., 2004; Carr et al., 2005; O'Brien et al., 2007*). Two separate digital fluxgate sensors will
925 perform magnetic field measurements. Fluxgate sensors are electrically passive and comprised of

SELMA: How do airless bodies interact with space environment?

926 magnetically susceptible cores, each core wrapped by two coils of wire. An alternating current is
927 passed through one coil (the drive coil), cyclically driving the core to positive and negative
928 magnetic saturation. A current proportional to the magnetic field along the coil axis is induced in
929 the other coil (the sense coil). In addition, a current is applied through the sense coil to directly
930 null the detected field along the coil axis through the magnetic core. The combination of current
931 through the three sense coils orthogonal to each other thus allows the full, local magnetic field
932 vector at each fluxgate sensor to be determined.

933 **4.9 Lunar Exospheric Mass Spectrometer (LEMS)**

934 The SELMA neutral gas mass spectrometer (LEMS) is a ToF mass spectrometer using an ion
935 mirror (reflectron) for performance optimization (*Wurz et al., 2012*). The LEMS mass range is 1–
936 1000 with the resolution of $M/\Delta M = 1100$. The dynamic range is at least 6 decades for a 5 s
937 integration period, allowing for the identification of species down to a partial density of about
938 1 cm^{-3} in such a measurement.

939 Ions are either generated in a storage ion source (neutral mode) or collected from the ambient
940 plasma (ion mode). With the pulsed ion optics of the ion source, ion packets are produced,
941 accelerated, shaped and sent into the ToF structure. After passing the first leg of a field-free drift
942 path, ions are reflected by an ion mirror, which allows energy and spatial focusing, and are then
943 directed onto a fast micro-channel plate detector. The charge signal versus time is recorded on the
944 detector, registered by a fast analogue-to-digital converter (ADC) system, and converted into a
945 mass spectrum. A ToF mass spectrometer has inherent advantages with respect to other mass
946 spectrometer concepts since it allows recording of a complete mass spectrum at once without the
947 necessity of scanning over the mass range of interest (*Wiley and McLaren, 1955*). This results in
948 superior efficiency over scanning instruments (i.e., magnetic sector instruments and quadrupole
949 mass analyzers) and is particularly useful during transient lunar phenomena, where only a short
950 time span is available to perform the mass spectrometric measurements. The LEMS design
951 benefits from heritage from the RTOF sensor of the ROSINA instrument on the Rosetta mission
952 as well as a stratospheric balloon in summer 2008 (*Abplanalp et al., 2009; Wieser et al., 2009b*).

953 **4.10 Plasma Wave Instrument (Orchestra)**

954 The instrument Orchestra will monitor the full electric field vector in the frequency range DC up
955 to 1.4 MHz, which will facilitate measurements of a wide range of plasma and electromagnetic
956 waves, including static electric structures, as well as monitoring signals for sampling
957 micrometeoroid impacts, and the spacecraft potential. In addition, Orchestra can also be run in
958 so-called Langmuir mode, and in so doing sample the cold plasma density and integrated EUV
959 flux. These parameters will provide the basis to a) characterize the electric field strength and
960 structure including related acceleration and energization processes within mini-magnetospheres
961 near surface of the Moon (e.g. acceleration structures, Alfvén or whistler wave processes, ion and
962 electron cyclotron waves, boundary processes, reconnection); b) characterize the ambient
963 size/mass distribution of μm -sized dust around the Moon; c) characterize the cold plasma
964 environment; and d) monitor the spacecraft potential for use by the particle instruments.

965 Two Langmuir probe sensors sample electric voltages or currents, which are the basis of the
966 inferred physical parameters. The probes can therefore be operated in two different modes:
967 current sampling mode (used as Langmuir probes) for plasma diagnostics (e.g., electron and ion
968 densities, electron temperature, and the drift speed) or voltage sampling mode (used as electric
969 field probes) for measurement of the electric field. The spacecraft potential is always measured
970 independent of operation mode. It is important to have both probes extended as far as possible

SELMA: How do airless bodies interact with space environment?

971 from each other and from spacecraft structures. The 3m long booms, properly accommodated,
972 facilitate this.

973 **4.11 Lunar Dust Detector (LDD)**

974 LDD is an *in situ* dust detector to map the variability of the spatial and size distribution of dust
975 near the Moon. It is a ‘built-to-print’ version of the Lunar Dust Experiment (LDEX) that flew
976 onboard NASA’s LADEE mission from September 2013 to April 2014 (*Horányi et al., 2015*).
977 LDD will provide complementary observations by a) verifying LDEX results; b) extending the
978 timeline of observations of the dust ejecta production during different meteoroid streams; c)
979 extending the spatial coverage using SELMA’s polar orbit; and d) enabling correlation studies
980 between dust influx/production, with the variability of the neutral and plasma environment to be
981 measured by the rest of the SELMA payload.

982 The detection of a dust particle is based on measuring the charge generated by its hypervelocity
983 ($v > 1 \text{ km s}^{-1}$) impact on a target. The impact charge Q (the total number of ions or electrons) is a
984 function of both the speed v , and the mass m , of the impacting dust particle

$$985 \quad Q = \alpha m v^\beta$$

986 where the charge is measured in C, the mass in kg, and the speed in km s^{-1} . The speed exponent
987 is in the range $3.5 \leq \beta \leq 5.6$. For a characteristic value of $\beta = 3.5$, $\alpha \sim 0.5$. The values for both α
988 and β are determined by calibrating individual instruments as they depend on the composition of
989 both the impactor and the target, and the geometry of the setup (*Horányi et al., 2014*).

990 **4.12 Waves and Electric field (MiniEF on SIP-MA)**

991 Mini-EF on board the SIP-MA makes use of similar electronics as the Orchestra instrument, but
992 different type of 4 booms and associated 4 Langmuir probe sensors. The MiniEF will use shorter
993 sticks (75 cm), smaller spheres and the pre-amplifiers are within the electric box but the operation
994 principle is similar to Orchestra instrument. MiniEF will not operate in Langmuir mode.

995 **4.13 Impact probe ions and electrons spectrometer (IPEI on SIP-MA)**

996 IPEI is going to measure the properties of the ions and electrons in the magnetic anomalies. The
997 design and the detection principle is the same as the LES instrument which is described above
998 (inverse polarities for the ion detector).

999 **4.14 Impact probe magnetometer (IPMAG on SIP-MA)**

1000 The SELMA Impact Probe Magnetometer IPMAG is based on the digital fluxgate magnetometer
1001 SMILE (e.g. *Forsslund et al, 2008, Belyayev and Ivchenko, 2015*). It is a miniature flux-gate
1002 system with volume compensation sensor, providing magnetic field measurements at a rate of up
1003 to 250 Hz, with 16-bit resolution. IPMAG is built around a digital implementation of the
1004 correlation loop, implemented in Field Programmable Field Array (FPGA), where the digital
1005 samples from the sense coils are processed in a matched filter to produce the digital value of the
1006 compensation current. The SMILE magnetometer has been flown on a number of sub-orbital
1007 flights (e.g. NASA’s Cascades-2 sounding rocket, SNSB’s SPIDER sounding rocket) and is
1008 qualified to fly on the SEAM nanosatellite in 2017 (realized as EU FP7 project under grant
1009 agreement 607197).

1010 The IPMAG instrument will consist of two three-axis fluxgate sensors mounted at different
1011 distances from the spacecraft on a 2 m long boom, and electronics inside the impactor. Using one
1012 boom for both sensors decreases the influence of spacecraft magnetic interference on the

SELMA: How do airless bodies interact with space environment?

1013 accuracy of the measurements. The 2 m long deployable boom for the two magnetometers is a
1014 modification of the dual-tip deployable boom for the SEAM satellite (Mao et al., 2017). Counter-
1015 rotating tape spring spools are deployed along with the boom tip. The IPMAG boom design uses
1016 the same type of tape springs and spools as the SEAM boom.

1017 **4.15 Context cameras (IPCAM on SIP-MA, IECAM on RCS)**

1018 IPCAM and IECAM are ordinary RGB cameras that will be mounted on SIP-MA and RCS for
1019 video streaming. The main objectives are the context imaging, helping to define the attitude
1020 determination, and PR purposes.

1021 **4.16 Impactor**

1022 The impactor for the impact experiment in the Shackleton crater is a copper sphere of 10 kg (13
1023 cm in diameter). The impactor is passive and does not carry any systems. The spherical shape
1024 ensures the independence of the impact on the impactor attitude. The copper is selected to
1025 identify the impactor's elements in the volatile plume.

1026 **5 Discussion and Summary**

1027 The SELMA mission investigating the interactions between the surface, exosphere, plasma and
1028 dust aims at a launch in 2029–2030 under the ESA's medium-size mission (M5) of the Cosmic
1029 Vision programme. SELMA addresses two Cosmic Vision themes; “1. What are the conditions
1030 for planet formation and the emergence of life?” and “2. How does the Solar System work?”
1031 (*Cosmic Vision, 2005*). In particular, SELMA focuses the Cosmic Vision topics “1.3 Life and
1032 habitability in the Solar System” and “2.3 Asteroids and other small bodies”.

1033 SELMA is a unique mission to investigate the complex local space environment–surface
1034 interactions. No missions with similar objectives and payload were, are, or will be conducted or
1035 planned in the near future. The NASA LADEE mission (Lunar Atmosphere, Dust Environment
1036 Explorer, 2013–2014) did not carry the full set of remote sensing instruments and plasma, field,
1037 and wave investigations. NASA ARTEMIS (two spacecraft for plasma and field measurements),
1038 which is currently in-orbit around the Moon, is not equipped with the instrumentation to
1039 characterize the surface properties, exosphere, and dust. Currently, the NASA LRO (Lunar
1040 Reconnaissance Orbiter) focuses on remote sensing but lack instrumentation for in situ and
1041 remote measurements of the local space environment. The Indian Chandrayaan-1 mission
1042 (October 2008 – August 2010) with ESA funded science payloads served as a pathfinder for the
1043 SELMA mission and demonstrated that the SELMA mission concept is feasible. SELMA will not
1044 only perform similar measurements using superior instruments, but it will also characterize the
1045 dynamic exosphere and dust environment.

1046 In term of the surface properties and the interaction with the environment, the Moon and Mercury
1047 are similar. Although the Mercury has global magnetic field, it has similar physical processes in
1048 terms of the interactions between exosphere, plasma and surface because of the lack of the
1049 atmosphere (e.g. Millilo et al., 2005; Lue et al., 2017). The influence of the plasma to the surface,
1050 which could vary, sputter and weather the surface does happen both at Moon and Mercury. Due
1051 to the different interplanetary dust particle speeds (Christou et al., 2015), the parameter range of
1052 the observations can be extended, and we can better know the effects of dust impacts on
1053 environment. From these comparative aspects into account, the Moon serves as a test-bed in the
1054 Earth's backyard to study these processes and better explore and understand the BepiColombo
1055 data. ESA BepiColombo will reach Mercury in 2024 and is planned to be operation until 2027.
1056 The active data analysis will continue for at least 5 years. The SELMA results, available in 2030,

SELMA: How do airless bodies interact with space environment?

1057 will come very timely to provide the key knowledge for BepiColombo data interpretation to
1058 understand the Mercury's exosphere and its variability, the role of the surface in refilling the
1059 magnetosphere via ion backscattering and sputtering, and the influence of the environment on the
1060 IR and UV surface characteristics. SELMA is a mission of comparative planetology.

1061 The impact experiments SELMA will perform are completely unique. Unprecedented fly-through
1062 of a mini-magnetosphere and high time resolution measurements down to the surface have never
1063 been even attempted before. The impact experiment in the permanently shadowed Shackleton
1064 crater is the first of its kind. The NASA LCROSS mission (Lunar Crater Observation and Sensing
1065 Satellite) in 2009 only used remote sensing to investigate the debris plume. SELMA will use in-
1066 situ instruments, in particular its powerful mass spectrometer, to directly sample volatiles
1067 released during the impact. Due to its position almost at the South Pole and sufficiently high rims,
1068 the Shackleton crater to be investigated by the SELMA impact experiment is one of the most
1069 interesting locations for future lunar exploration missions.

1070 Research on the SELMA scientific theme is of importance for both fundamental planetary
1071 sciences, for our general understanding of how the Solar System works, and for future lunar
1072 explorations, through qualitative characterization of the lunar environment and, in particular,
1073 investigation of the presence of water in the lunar soil, as a valuable resource to harvest from the
1074 lunar regolith. Determining the water content in the crater's soil is critical for decisions on South
1075 Pole exploration.

1076 **Acknowledgement**

1077 The SELMA proposal team acknowledges the financial support from the Swedish National Space
1078 Board (SNSB) for the mission analysis conducted by OHB, Sweden.

1079 **References**

- 1080 Abplanalp, D., P. Wurz, L. Huber, I. Leya, E. Kopp, U. Rohner, M. Wieser, L. Kalla, and
1081 S. Barabash, A neutral gas mass spectrometer to measure the chemical composition of the
1082 stratosphere, *Adv. Space Res.*, 44(7), 870–878, doi: 10.1016/j.asr.2009.06.016, 2009.
- 1083 Anderson, B. J., C. L. Johnson, H. Korth, M. E. Purucker, R. M. Winslow, J. A. Slavin, S. C.
1084 Solomon, R. L. McNutt, J. M. Raines, and T. H. Zurbuchen, The global magnetic field of
1085 Mercury from Messenger orbital observations, *Science*, 333(6051), 1859–1862,
1086 doi:10.1126/science.1211001, 2011.
- 1087 Arnold, J. R., Ice in the lunar polar regions, *J. Geophys. Res.*, 84(B10), 5659–5668,
1088 doi: 10.1029/JB084iB10p05659, 1979.
- 1089 Barabash, S., A. Bhardwaj, M. Wieser, R. Sridharan, T. Kurian, S. Varier, E. Vijaykumar,
1090 V. Abhirami, K. V. Raghavendra, S. V. Mohankumar, D. B. Dhanya, S. Thampi,
1091 K. Asamura, H. Andersson, Y. Futaana, M. Holmström, R. Lundin, J. Svensson,
1092 S. Karlsson, R. D. Piazza, and P. Wurz, Investigation of the solar wind-Moon interaction
1093 on board Chandrayaan-1 mission with the SARA experiment, *Current Science*, 96(4), 526–
1094 532, 2009.
- 1095 Bellot Rubio, L. R., J. L. Ortiz, and P. V. Sada, Observation and interpretation of meteoroid
1096 impact flashes on the moon, in *Leonid Storm Research*, edited by P. Jenniskens,
1097 F. Rietmeijer, N. Brosch, and M. Fonda, pp. 575–598, Springer Netherlands, Dordrecht,
1098 doi: 10.1007/978-94-017-2071-7_42, 2000.
- 1099 Belyayev, S., and N. Ivchenko, Digital fluxgate magnetometer: design notes, *Meas. Sci. Technol.*,
1100 26(12), 125,901, doi: 10.1088/0957-0233/26/12/125901, 2015.

SELMA: How do airless bodies interact with space environment?

- 1101 Benna, M., P. R. Mahaffy, J. S. Halekas, R. C. Elphic, and G. T. Delory, Variability of helium,
1102 neon, and argon in the lunar exosphere as observed by the LADEE NMS instrument,
1103 *Geophys. Res. Lett.*, 42(10), 3723–3729, doi: 10.1002/2015GL064120, 2015.
- 1104 Berg, O., H. Wolf, and J. Rhee, Lunar soil movement registered by the Apollo 17 cosmic dust
1105 experiment, in *Interplanetary Dust and Zodiacal Light, Lecture Notes in Physics*, vol. 48,
1106 edited by H. Elsässer and H. Fechting, pp. 233–237, Springer Berlin / Heidelberg,
1107 doi: 10.1007/3-540-07615-8_486, 1976.
- 1108 Bruck Syal, M., and P. H. Schultz, Cometary impact effects at the moon: Implications for lunar
1109 swirl formation, *Icarus*, 257, 194–206, doi: 10.1016/j.icarus.2015.05.005, 2015.
- 1110 Carr, C., P. Brown, T. L. Zhang, J. Gloag, T. Horbury, E. Lucek, W. Magnes, H. O’Brien,
1111 T. Oddy, U. Auster, P. Austin, O. Aydogar, A. Balogh, W. Baumjohann, T. Beek,
1112 H. Eichelberger, K.-H. Fornacon, E. Georgescu, K.-H. Glassmeier, M. Ludlam,
1113 R. Nakamura, and I. Richter, The Double Star magnetic field investigation: instrument
1114 design, performance and highlights of the first year’s observations, *Ann. Geophys.*, 23(8),
1115 2713–2732, doi: 10.5194/angeo-23-2713-2005, 2005.
- 1116 Christou, A. A., R. M. Killen, and M. H. Burger, The meteoroid stream of comet Encke at
1117 Mercury: Implications for Mercury Surface, Space Environment, Geochemistry, and
1118 Ranging observations of exosphere, *Geophys. Res. Lett.*, 42, 7311–7318,
1119 doi:10.1002/2015GL065361, 2015.
- 1120 Clark, R. N., Detection of adsorbed water and hydroxyl on the Moon, *Science*, 326(5952), 562–
1121 564, doi: 10.1126/science.1178105, 2009.
- 1122 Cocks, F. H., P. A. Klenk, S. A. Watkins, W. N. Simmons, J. C. Cocks, E. E. Cocks, and J. C.
1123 Sussingham, Lunar ice: Adsorbed water on subsurface polar dust, *Icarus*, 160(2), 386–397,
1124 doi: 10.1006/icar.2002.6972, 2002.
- 1125 Colaprete, A., P. Schultz, J. Heldmann, D. Wooden, M. Shirley, K. Ennico, B. Hermalyn,
1126 W. Marshall, A. Ricco, R. C. Elphic, D. Goldstein, D. Summy, G. D. Bart, E. Asphaug,
1127 D. Korycansky, D. Landis, and L. Sollitt, Detection of water in the LCROSS ejecta plume,
1128 *Science*, 330(6003), 463–468, doi: 10.1126/science.1186986, 2010.
- 1129 Coleman Jr., P. J., C. T. Russel, L. R. Sharp, and G. Schubert, Preliminary mapping of the lunar
1130 magnetic field, *Phys. Earth Planet. Interiors*, 6, 167–174, doi: 10.1016/0031-
1131 9201(72)90050-7, 1972.
- 1132 Cook, J. C., and S. Alan Stern, Sporadic increases in lunar atmospheric helium detected by lamp,
1133 *Icarus*, 236, 48–55, doi: 10.1016/j.icarus.2014.02.001, 2014.
- 1134 Cook, J. C., S. A. Stern, P. D. Feldman, G. R. Gladstone, K. D. Retherford, and C. C. C. Tsang,
1135 New upper limits on numerous atmospheric species in the native lunar atmosphere, *Icarus*,
1136 225(1), 681–687, doi: 10.1016/j.icarus.2013.04.010, 2013.
- 1137 Crider, D. H., and R. R. Vondrak, The solar wind as a possible source of lunar polar hydrogen
1138 deposits, *J. Geophys. Res.*, 105(E11), 26,773–26,782, doi: 10.1029/2000JE001277, 2000.
- 1139 Crider, D. H., and R. R. Vondrak, Hydrogen migration to the lunar poles by solar wind
1140 bombardment of the Moon, *Adv. Space Res.*, 30(8), 1869–1874, doi: 10.1016/S0273-
1141 1177(02)00493-3, 2002.
- 1142 Crider, D. H., and R. R. Vondrak, Space weathering effects on lunar cold trap deposits, *J.*
1143 *Geophys. Res.*, 108(E7), 5079, doi: 10.1029/2002JE002030, 2003.
- 1144 Criswell, D. R., Horizon-glow and the motion of lunar dust, in *Photon and particle interactions*
1145 *with surfaces in space*, edited by R. J. L. Grard, Springer, doi: 10.1007/978-94-010-2647-
1146 5\do5(3)6, 1973.
- 1147 Deca, J., A. Divin, B. Lembège, M. Horányi, S. Markidis, and G. Lapenta, General mechanism
1148 and dynamics of the solar wind interaction with lunar magnetic anomalies from 3-d
1149 particle-in-cell simulations, *J. Geophys. Res.*, 120(8), 6443–6463,
1150 doi: 10.1002/2015JA021070, 2015.

SELMA: How do airless bodies interact with space environment?

- 1151 Dougherty, M. K., S. Kellock, D. J. Southwood, a. Balogh, E. J. Smith, B. T. Tsurutani,
1152 B. Gerlach, K.-H. Glassmeier, F. Gleim, C. T. Russell, G. Erdos, F. M. Neubauer, and
1153 S. W. H. Cowley, The Cassini magnetic field investigation, *Space Sci. Rev.*, *114*(1-4), 331–
1154 383, doi: 10.1007/s11214-004-1432-2, 2004.
- 1155 Dyadechkin, S., Kallio, E., Wurz, P., New fully kinetic model for the study of electric potential,
1156 plasma, and dust above lunar landscapes. *J. Geophys. Res.* *120* (3), 1589–1606,
1157 doi:10.1002/2014JA020511, 2015.
- 1158 Dyal, P., C. W. Parkin, and C. P. Sonett, Apollo 12 magnetometer: Measurement of a steady
1159 magnetic field on the surface of the moon, *Science*, *169*(3947), 762–764,
1160 doi: 10.1126/science.169.3947.762, 1970.
- 1161 Elphic, R. C., B. Hine, G. T. Delory, J. S. Salute, S. Noble, A. Colaprete, M. Horanyi,
1162 P. Mahaffy, and the LADEE Science Team, The lunar atmosphere and dust environment
1163 explorer (LADEE): Initial science results., in *45th Lunar and Planetary Science*
1164 *Conference*, p. 2677, 2014.
- 1165 Fatemi, S., M. Holmström, Y. Futaana, C. Lue, M. R. Collier, S. Barabash, and G. Stenberg,
1166 Effects of protons reflected by lunar crustal magnetic fields on the global lunar plasma
1167 environment, *J. Geophys. Res.*, doi: 10.1002/2014JA019900, 2014.
- 1168 Fatemi, S., C. Lue, M. Holmström, A. R. Poppe, M. Wieser, S. Barabash, and G. T. Delory, Solar
1169 wind plasma interaction with Gerasimovich lunar magnetic anomaly, *J. Geophys. Res.*,
1170 *120*(6), 4719–4735, doi: 10.1002/2015JA021027, 2015.
- 1171 Feldman, P. D., D. M. Hurley, K. D. Retherford, G. R. Gladstone, S. A. Stern, W. Pryor, J. W.
1172 Parker, D. E. Kaufmann, M. W. Davis, and M. H. Versteeg, Temporal variability of lunar
1173 exospheric helium during January 2012 from LRO/LAMP, *Icarus*, *221*(2), 854–858,
1174 doi: 10.1016/j.icarus.2012.09.015, 2012.
- 1175 Feldman, P. D., D. A. Glenar, T. J. Stubbs, K. D. Retherford, G. Randall Gladstone, P. F. Miles,
1176 T. K. Greathouse, D. E. Kaufmann, J. W. Parker, and S. Alan Stern, Upper limits for a
1177 lunar dust exosphere from far-ultraviolet spectroscopy by LRO/LAMP, *Icarus*, *233*, 106–
1178 113, doi: 10.1016/j.icarus.2014.01.039, 2014.
- 1179 Feldman, W. C., S. Maurice, A. B. Binder, B. L. Barraclough, R. C. Elphic, and D. J. Lawrence,
1180 Fluxes of fast and epithermal neutrons from Lunar Prospector: Evidence for water ice at the
1181 lunar poles, *Science*, *281*(5382), 1496–1500, doi: 10.1126/science.281.5382.1496, 1998.
- 1182 Flynn, B., and M. Mendillo, A picture of the Moon's atmosphere, *Science*, *261*(5118), 184–186,
1183 doi: 10.1126/science.261.5118.184, 1993.
- 1184 Forslund, Å., S. Belyayev, N. Ivchenko, G. Olsson, T. Edberg, and A. Marusenkov, Miniaturized
1185 digital fluxgate magnetometer for small spacecraft applications, *Meas. Sci. Technol.*, *19*(1),
1186 015,202, doi: 10.1088/0957-0233/19/1/015202, 2008.
- 1187 Futaana, Y., S. Barabash, M. Wieser, M. Holmström, C. Lue, P. Wurz, A. Schaufelberger,
1188 A. Bhardwaj, M. B. Dhanya, and K. Asamura, Empirical energy spectra of neutralized
1189 solar wind protons from the lunar regolith, *J. Geophys. Res.*, *117*(E5), E05005,
1190 doi: 10.1029/2011JE004019, 2012.
- 1191 Futaana, Y., S. Barabash, M. Wieser, C. Lue, P. Wurz, A. Vorburger, A. Bhardwaj, and
1192 K. Asamura, Remote energetic neutral atom imaging of electric potential over a lunar
1193 magnetic anomaly, *Geophys. Res. Lett.*, *40*, 262–266, doi: 10.1002/grl.50135, 2013.
- 1194 Garrick-Bethell, I., J. W. Head III, and C. M. Pieters, Spectral properties, magnetic fields, and
1195 dust transport at lunar swirls, *Icarus*, *212*(2), 480 – 492, doi: 10.1016/j.icarus.2010.11.036,
1196 2011.
- 1197 Gladstone, G. R., S. A. Stern, K. D. Retherford, R. K. Black, D. C. Slater, M. W. Davis, M. H.
1198 Versteeg, K. B. Persson, J. W. Parker, D. E. Kaufmann, A. F. Egan, T. K. Greathouse,
1199 P. D. Feldman, D. Hurley, W. R. Pryor, and A. R. Hendrix, LAMP: The Lyman alpha

SELMA: How do airless bodies interact with space environment?

- 1200 mapping project on NASA's Lunar Reconnaissance Orbiter mission, *Space Sci. Rev.*,
1201 150(1), 161–181, doi: 10.1007/s11214-009-9578-6, 2010.
- 1202 Gladstone, G. R., K. D. Retherford, A. F. Egan, D. E. Kaufmann, P. F. Miles, J. W. Parker,
1203 D. Horvath, P. M. Rojas, M. H. Versteeg, M. W. Davis, T. K. Greathouse, D. C. Slater,
1204 J. Mukherjee, A. J. Steffl, P. D. Feldman, D. M. Hurley, W. R. Pryor, A. R. Hendrix,
1205 E. Mazarico, and S. A. Stern, Far-ultraviolet reflectance properties of the Moon's
1206 permanently shadowed regions, *J. Geophys. Res.*, 117, doi: 10.1029/2011JE003913, 2012.
- 1207 Glenar, D. A., T. J. Stubbs, J. M. Hahn, and Y. Wang, Search for a high-altitude lunar dust
1208 exosphere using clementine navigational star tracker measurements, *J. Geophys. Res.*,
1209 119(12), 2548–2567, doi: 10.1002/2014JE004702, 2014.
- 1210 Grava, C., K. D. Retherford, D. M. Hurley, P. D. Feldman, G. R. Gladstone, T. K. Greathouse,
1211 J. C. Cook, S. A. Stern, W. R. Pryor, J. S. Halekas, and D. E. Kaufmann, Lunar exospheric
1212 helium observations of LRO/LAMP coordinated with ARTEMIS, *Icarus*, 273, 36–44,
1213 doi: 10.1016/j.icarus.2015.10.033, 2016.
- 1214 Grün, E., H. A. Zook, H. Fechtig, and R. H. Giese, Collisional balance of the meteoritic complex,
1215 *Icarus*, 62(2), 244–272, doi: 10.1016/0019-1035(85)90121-6, 1985.
- 1216 Grün, E., M. Horanyi, and Z. Sternovsky, The lunar dust environment, *Planet. Space Sci.*, 59(14),
1217 1672–1680, doi: 10.1016/j.pss.2011.04.005, 2011.
- 1218 Halekas, J., G. Delory, D. Brain, R. Lin, and D. Mitchell, Density cavity observed over a strong
1219 lunar crustal magnetic anomaly in the solar wind: A mini-magnetosphere?, *Planet. Space*
1220 *Sci.*, 56(7), 941–946, doi: 10.1016/j.pss.2008.01.008, 2008.
- 1221 Halekas, J. S., A. R. Poppe, G. T. Delory, M. Sarantos, and J. P. McFadden, Using ARTEMIS
1222 pickup ion observations to place constraints on the lunar atmosphere, *J. Geophys. Res.*,
1223 118(1), 81–88, doi: 10.1029/2012JE004292, 2013.
- 1224 Halekas, J. S., M. Benna, P. R. Mahaffy, R. C. Elphic, A. R. Poppe, and G. T. Delory, Detections
1225 of lunar exospheric ions by the LADEE neutral mass spectrometer, *Geophys. Res. Lett.*,
1226 42(13), 5162–5169, doi: 10.1002/2015GL064746, 2015.
- 1227 Hartle, R. E., and R. Killen, Measuring pickup ions to characterize the surfaces and exospheres of
1228 planetary bodies: Applications to the Moon, *Geophys. Res. Lett.*, 33(5), n/a–n/a,
1229 doi: 10.1029/2005GL024520, 2006.
- 1230 Heiken, G. H., D. T. Vaniman, and B. M. French (Eds.), *Lunar sourcebook: a user's guide to the*
1231 *moon*, Cambridge University Press, 1991.
- 1232 Hendrix, A. R., K. D. Retherford, G. Randall Gladstone, D. M. Hurley, P. D. Feldman, A. F.
1233 Egan, D. E. Kaufmann, P. F. Miles, J. W. Parker, D. Horvath, P. M. Rojas, M. H. Versteeg,
1234 M. W. Davis, T. K. Greathouse, J. Mukherjee, A. J. Steffl, W. R. Pryor, and S. A. Stern,
1235 The lunar far-UV albedo: Indicator of hydration and weathering, *J. Geophys. Res.*,
1236 117(E12), n/a–n/a, doi: 10.1029/2012JE004252, 2012.
- 1237 Hinton, F., and D. Taesch, Variation of the lunar atmosphere with the strength of the solar wind,
1238 *J. Geophys. Res.*, 69(7), 1341–1347, doi: 10.1029/JZ069i007p01341, 1964.
- 1239 Hodges, J., R. Richard, Ice in the lunar polar regions revisited, *J. Geophys. Res.*, 107(E2),
1240 doi: 10.1029/2000JE001491, 2002.
- 1241 Hodges, R. R., Exospheric transport restrictions on water ice in lunar polar traps, *Geophys. Res.*
1242 *Lett.*, 18(11), 2113–2116, doi: 10.1029/91GL02533, 1991.
- 1243 Hodges, R. R., Resolution of the lunar hydrogen enigma, *Geophys. Res. Lett.*, 38, L06201,
1244 doi: 10.1029/2011GL046688, 2011.
- 1245 Hodges, R. R., Methane in the lunar exosphere: Implications for solar wind carbon escape,
1246 *Geophys. Res. Lett.*, 43(13), 6742–6748, doi: 10.1002/2016GL068994, 2016.
- 1247 Hodges, R. R., and F. S. Johnson, Lateral transport in planetary exospheres, *J. Geophys. Res.*,
1248 73(23), 7307–7317, doi: 10.1029/JA073i023p07307, 1968.

SELMA: How do airless bodies interact with space environment?

- 1249 Hodges, R. R., Jr., and J. H. Hoffman, Implications of atmospheric Ar-40 escape on the interior
1250 structure of the moon, in *Lunar and Planetary Science Conference Proceedings, Lunar and*
1251 *Planetary Science Conference Proceedings*, vol. 6, pp. 3039–3047, 1975.
- 1252 Hodges, R. R. J., J. H. Hoffman, F. S. Johnson, and D. E. Evans, Composition and dynamics of
1253 lunar atmosphere, in *Lunar and Planetary Science Conference Proceedings*, 1142, pp. 374–
1254 375, 1973.
- 1255 Hood, L. L., and Z. Huang, Formation of magnetic anomalies antipodal to lunar impact basins:
1256 Two-dimensional model calculations, *J. Geophys. Res.*, 96(B6), 9837–9846,
1257 doi: 10.1029/91JB00308, 1991.
- 1258 Hood, L. L., P. J. Coleman, Jr., and D. E. Wilhelms, Lunar nearside magnetic anomalies, in
1259 *Lunar and Planetary Science Conference Proceedings, Lunar and Planetary Science*
1260 *Conference Proceedings*, vol. 10, edited by N. W. Hinners, pp. 2235–2257, 1979.
- 1261 Hood, L. L., A. Zakharian, J. Halekas, D. L. Mitchell, R. P. Lin, M. H. Acuña, and A. B. Binder,
1262 Initial mapping and interpretation of lunar crustal magnetic anomalies using Lunar
1263 Prospector magnetometer data, *J. Geophys. Res.*, 106(E11), 27,825–27,839,
1264 doi: 10.1029/2000JE001366, 2001.
- 1265 Horányi, M., Z. Sternovsky, M. Lankton, C. Dumont, S. Gagnard, D. Gathright, E. Grün,
1266 D. Hansen, D. James, S. Kempf, B. Lamprecht, R. Srama, J. R. Szalay, and G. Wright, The
1267 lunar dust experiment (LDEX) onboard the lunar atmosphere and dust environment
1268 explorer (LADEE) mission, *Space Sci. Rev.*, 185(1), 93–113, doi: 10.1007/s11214-014-
1269 0118-7, 2014.
- 1270 Horanyi, M., J. R. Szalay, S. Kempf, J. Schmidt, E. Grun, R. Srama, and Z. Sternovsky, A
1271 permanent, asymmetric dust cloud around the Moon, *Nature*, 522(7556), 324–326,
1272 doi: 10.1038/nature14479, 2015.
- 1273 Housen, K. R., and K. A. Holsapple, Ejecta from impact craters, *Icarus*, 211(1), 856–875,
1274 doi: 10.1016/j.icarus.2010.09.017, 2011.
- 1275 Hunten, D. M., G. Cremonese, A. L. Sprague, R. E. Hill, S. Verani, and R. W. H. Kozlowski, The
1276 Leonid meteor shower and the lunar sodium atmosphere, *Icarus*, 136(2), 298–303,
1277 doi: 10.1006/icar.1998.6023, 1998.
- 1278 Hurley, D. M., J. C. Cook, M. Benna, J. S. Halekas, P. D. Feldman, K. D. Retherford, R. R.
1279 Hodges, C. Grava, P. Mahaffy, G. R. Gladstone, T. Greathouse, D. E. Kaufmann, R. C.
1280 Elphic, and S. A. Stern, Understanding temporal and spatial variability of the lunar helium
1281 atmosphere using simultaneous observations from LRO, LADEE, and ARTEMIS, *Icarus*,
1282 273, 45–52, doi: 10.1016/j.icarus.2015.09.011, 2016.
- 1283 Hurley, D. M., J. C. Cook, K. D. Retherford, T. Greathouse, G. R. Gladstone, K. Mandt,
1284 C. Grava, D. Kaufmann, A. Hendrix, P. D. Feldman, W. Pryor, A. Stickle, R. M. Killen,
1285 and S. A. Stern, Contributions of solar wind and micrometeoroids to molecular hydrogen in
1286 the lunar exosphere, *Icarus*, pp. 31–37, doi: 10.1016/j.icarus.2016.04.019, 2017.
- 1287 Iglseider, H., K. Uesugi, and H. Svedhem, Cosmic dust measurements in lunar orbit, *Adv. Space*
1288 *Res.*, 17(12), 177–182, doi: 10.1016/0273-1177(95)00777-C, 1996.
- 1289 Imamura, T., T. Iwata, Z. ichi Yamamoto, N. Mochizuki, Y. Kono, K. Matsumoto, Q. Liu,
1290 H. Noda, H. Harada, K. ichiro Oyama, A. Nabatov, Y. Futaana, A. Saito, and H. Ando,
1291 Studying the lunar ionosphere with SELENE Radio Science experiment, *Space Sci. Rev.*,
1292 doi: 10.1007/s11214-010-9660-0, 2010.
- 1293 Jarvinen, R., M. Alho, E. Kallio, P. Wurz, S. Barabash, and Y. Futaana, On vertical electric fields
1294 at lunar magnetic anomalies, *Geophys. Res. Lett.*, 41(7), 2243–2249,
1295 doi: 10.1002/2014GL059788, 2014.
- 1296 Johnson, F. S., Lunar atmosphere, *Rev. Geophys.*, 9(3), 813–823,
1297 doi: 10.1029/RG009i003p00813, 1971.

SELMA: How do airless bodies interact with space environment?

- 1298 Kallio, E., R. Jarvinen, S. Dyadechkin, P. Wurz, S. Barabash, F. Alvarez, V. A. Fernandes, Y.
1299 Futaana, A.-M. Harri, J. Heilimo, C. Lue, J. Mäkelä, N. Porjo, W. Schmidt, and T. Siili,
1300 Kinetic simulations of finite gyroradius effects in the lunar plasma environment on global,
1301 meso, and microscales, *Planet. Space Sci.*, *74*(1), 146–155, doi:10.1016/j.pss.2012.09.012,
1302 2012.
- 1303 Kallio, E., S. Dyadechkin, S. Fatemi, M. Holmström, Y. Futaana, P. Wurz, V. A. Fernandes, F.
1304 Álvarez, J. Heilimo, R. Jarvinen, W. Schmidt, A. M. Harri, S. Barabash, J. Mäkelä, N.
1305 Porjo, and M. Alho, Dust environment of an airless object: A phase space study with
1306 kinetic models, *Planet. Space Sci.*, *120*, 56–69, doi:10.1016/j.pss.2015.11.006, 2016.
- 1307 Killen, R. M., M. H. Burger, and W. M. Farrell, Exospheric escape: A parametrical study, *Adv.*
1308 *Space Res.*, doi:10.1016/j.asr.2017.06.015, in Press.
- 1309 Kirsch, E., B. Wilken, G. Gloeckler, A. Galvin, J. Geiss, and D. Hovestadt, Search for lunar
1310 pickup ions, in *COSPAR Colloquia Series*, vol. 9, pp. 65–69, Elsevier, doi: 10.1016/S0964-
1311 2749(98)80011-5, 1998.
- 1312 Krüger, H., A. Krivov, and E. Grün, A dust cloud of Ganymede maintained by hypervelocity
1313 impacts of interplanetary micrometeoroids, *Planet. Space Sci.*, *48*(15), 1457–1471,
1314 doi: 10.1016/S0032-0633(00)00092-1, 2000.
- 1315 Lanzerotti, L. J., W. L. Brown, and R. E. Johnson, Ice in the polar regions of the moon, *J.*
1316 *Geophys. Res.*, *86*(B5), 3949–3950, doi: 10.1029/JB086iB05p03949, 1981.
- 1317 Li, S., R. E. Milliken, Water on the surface of the Moon as seen by the Moon Mineralogy
1318 Mapper: Distribution, abundance, and origins, *Sci. Adv.*, *3*, e1701471,
1319 doi:10.1126/sciadv.1701471, 2017.
- 1320 Lin, R. P., D. L. Mitchell, D. W. Curtis, K. A. Anderson, C. W. Carlson, J. McFadden, M. H.
1321 Acuña, L. L. Hood, and A. Binder, Lunar surface magnetic fields and their interaction with
1322 the solar wind: Results from Lunar Prospector, *Science*, *281*(5382), 1480–1484,
1323 doi: 10.1126/science.281.5382.1480, 1998.
- 1324 Lord, H. C., Hydrogen and helium ion implantation into olivine and enstatite: Retention
1325 coefficients, saturation concentrations, and temperature-release profiles, *J. Geophys. Res.*,
1326 *73*(16), 5271–5280, 1968.
- 1327 Lue, C., Y. Futaana, S. Barabash, M. Wieser, M. Holmström, A. Bhardwaj, M. Dhanya, and
1328 P. Wurz, Strong influence of lunar crustal fields on the solar wind flow, *Geophys. Res.*
1329 *Lett.*, *38*(3), L03202, doi: 10.1029/2010GL046215, 2011.
- 1330 Lue, C., Y. Futaana, S. Barabash, M. Wieser, A. Bhardwaj, and P. Wurz, Chandrayaan-1
1331 observations of backscattered solar wind protons from the lunar regolith: Dependence on
1332 the solar wind speed, *J. Geophys. Res.*, *119*, 968–975, doi: 10.1002/2013JE004582, 2014.
- 1333 Lue, C., Y. Futaana, S. Barabash, M. Wieser, A. Bhardwaj, P. Wurz, and K. Asamura, Solar wind
1334 scattering from the surface of Mercury: Lessons from the Moon, *Icarus*, *296*, 39–48,
1335 doi:10.1016/j.icarus.2017.05.019, 2017.
- 1336 Mall, U., E. Kirsch, K. Cierpka, B. Wilken, A. Söding, F. Neubauer, G. Gloeckler, and A. Galvin,
1337 Direct observation of lunar pick-up ions near the Moon, *Geophys. Res. Lett.*, *25*(20), 3799–
1338 3802, doi: 10.1029/1998GL900003, 1998.
- 1339 Mall, U., M. Banaszkiwicz, K. Brønstad, S. McKenna-Lawlor, A. Nathues, F. Søråas,
1340 E. Vilenius, and K. Ullaland, Near infrared spectrometer SIR-2 on Chandrayaan-1, *Current*
1341 *Science*, *96*(4), 506–511, 2009.
- 1342 Mangano, V., A. Milillo, A. Mura, S. Orsini, E. De Angelis, A. M. Di Lellis, and P. Wurz, The
1343 contribution of impulsive meteoritic impact vapourization to the Hermean exosphere,
1344 *Planet. Space Sci.*, *55*(11), 1541–1556, doi: 10.1016/j.pss.2006.10.008, 2007.
- 1345 Mao, H., P. L. Ganga, M. Ghiozzi, N. Ivchenko, and G. Tibert, Deployment of bistable self-
1346 deployable tape spring booms using a gravity offloading system, *J. Aerospace Eng.*, *30*(4),
1347 04017,007, doi: 10.1061/(ASCE)AS.1943-5525.0000709, 2017.

SELMA: How do airless bodies interact with space environment?

- 1348 McCord, T. B., L. A. Taylor, J. P. Combe, G. Kramer, C. M. Pieters, J. M. Sunshine, and R. N.
1349 Clark, Sources and physical processes responsible for OH/H₂O in the lunar soil as revealed
1350 by the Moon Mineralogy Mapper (M3), *J. Geophys. Res.*, *116*, E00G05,
1351 doi: 10.1029/2010JE003711, 2011.
- 1352 McCoy, J. E., Photometric studies of light scattering above the lunar terminator from Apollo solar
1353 corona photography, in *Proc. Lunar Sci. Conf. 7th*, pp. 1087–1112, 1976.
- 1354 McCoy, J. E., and D. R. Criswell, Evidence for a high altitude distribution of lunar dust, in
1355 *Proceedings of the Fifth Lunar Conference, Supplement 5, Ceochimica et Cosmochimica*
1356 *Acta*, vol. 3, pp. 2991–3005, 1974.
- 1357 Mendillo, M., and J. Baumgardner, Constraints on the origin of the Moon's atmosphere from
1358 observations during a lunar eclipse, *Nature*, *377*(6548), 404–406, doi: 10.1038/377404a0,
1359 1995.
- 1360 Milillo, A., P. Wurz, S. Orsini, D. Delcourt, E. Kallio, R. M. KILLEN, H. Lammer, S. Massetti,
1361 A. Mura, S. Barabash, G. Cremonese, I. A. Daglis, E. Angelis, A. M. Lellis, S. Livi, V.
1362 Mangano, and K. Torkar, Surface-exosphere-magnetosphere system of Mercury, *Space Sci.*
1363 *Rev.*, *117*(3), 397–443, doi:10.1007/s11214-005-3593-z, 2005.
- 1364 Mitrofanov, I. G., A. B. Sanin, W. V. Boynton, G. Chin, J. B. Garvin, D. Golovin, L. G. Evans,
1365 K. Harshman, A. S. Kozyrev, M. L. Litvak, A. Malakhov, E. Mazarico, T. McClanahan,
1366 G. Milikh, M. Mokrousov, G. Nandikotkur, G. A. Neumann, I. Nuzhdin, R. Sagdeev,
1367 V. Shevchenko, V. Shvetsov, D. E. Smith, R. Starr, V. I. Tretyakov, J. Trombka,
1368 D. Usikov, A. Varenikov, A. Vostrukhin, and M. T. Zuber, Hydrogen mapping of the lunar
1369 south pole using the LRO neutron detector experiment LEND, *Science*, *330*(6003), 483–
1370 486, doi: 10.1126/science.1185696, 2010.
- 1371 Murphy, D., and R. Vondrak, Effects of levitated dust on astronomical observations from the
1372 lunar surface, *American Astronomical Society, 182nd AAS Meeting, id.51.21; Bulletin of*
1373 *the American Astronomical Society*, *25*, 1033, 1993.
- 1374 Ness, N. F., K. W. Behannon, R. P. Lepping, Y. C. Whang, and K. H. Schatten, Magnetic field
1375 observations near Mercury: Preliminary results from Mariner 10, *Science*, *185*(4146), 151–
1376 160, doi: 10.1126/science.185.4146.151, 1974.
- 1377 Oberst, J., J. Flohrer, S. Elgner, T. Maue, A. Margonis, R. Schrödter, W. Tost, M. Buhl,
1378 J. Ehrich, A. Christou, and D. Koschny, The smart panoramic optical sensor head
1379 (SPOSH)—a camera for observations of transient luminous events on planetary night sides,
1380 *Planet. Space Sci.*, *59*(1), 1–9, doi: 10.1016/j.pss.2010.09.016, 2011.
- 1381 O'Brien, H., P. Brown, T. Beek, C. Carr, E. Cupido, and T. Oddy, A radiation tolerant digital
1382 fluxgate magnetometer, *Meas. Sci. Technol.*, *18*(11), 3645, doi: 10.1088/0957-
1383 0233/18/11/050, 2007.
- 1384 Ong, L., E. I. Asphaug, D. Korycansky, and R. F. Coker, Volatile retention from cometary
1385 impacts on the Moon, *Icarus*, *207*(2), 578–589, doi: 10.1016/j.icarus.2009.12.012, 2010.
- 1386 Pieters, C. M., J. N. Goswami, R. N. Clark, M. Annadurai, J. Boardman, B. Buratti, J. P. Combe,
1387 M. D. Dyar, R. Green, J. W. Head, C. Hibbitts, M. Hicks, P. Isaacson, R. Klima,
1388 G. Kramer, S. Kumar, E. Livo, S. Lundeen, E. Malaret, T. McCord, J. Mustard, J. Nettles,
1389 N. Petro, C. Runyon, M. Staid, J. Sunshine, L. A. Taylor, S. Tompkins, and P. Varanasi,
1390 Character and spatial distribution of OH/H₂O on the surface of the Moon seen by M3 on
1391 Chandrayaan-1, *Science*, *326*(5952), 568–572, doi: 10.1126/science.1178658, 2009.
- 1392 Poppe, A. R., S. Fatemi, I. Garrick-Bethell, D. Hemingway, and M. Holmström, Solar wind
1393 interaction with the reiner gamma crustal magnetic anomaly: Connecting source
1394 magnetization to surface weathering, *Icarus*, *266*, 261–266,
1395 doi: 10.1016/j.icarus.2015.11.005, 2016.
- 1396 Potter, A., and T. Morgan, Discovery of sodium and potassium vapor in the atmosphere of the
1397 Moon, *Science*, *241*(4866), 675–680, doi: 10.1126/science.241.4866.675, 1988.

SELMA: How do airless bodies interact with space environment?

- 1398 Potter, A., and T. Morgan, Coronagraphic observations of the lunar sodium exosphere near the
1399 lunar surface, *J. Geophys. Res.*, *103*(E4), 8581–8586, doi: 10.1029/98JE00059, 1998.
- 1400 Purucker, M. E., J. W. Head, and L. Wilson, Magnetic signature of the lunar south pole-aitken
1401 basin: Character, origin, and age, *J. Geophys. Res.*, *117*(E5), doi: 10.1029/2011JE003922,
1402 2012.
- 1403 Rennilson, J., and D. R. Criswell, Surveyor observations of lunar horizon-glow, *Earth, Moon,*
1404 *and Planets*, *10*, 121–142, doi: 10.1007/BF00655715, 1974.
- 1405 Richmond, N. C., and L. L. Hood, A preliminary global map of the vector lunar crustal magnetic
1406 field based on Lunar Prospector magnetometer data, *J. Geophys. Res.*, *113*(E2),
1407 doi: 10.1029/2007JE002933, 2008.
- 1408 Russell, C. T., and B. R. Lichtenstein, On the source of lunar limb compressions, *J. Geophys.*
1409 *Res.*, *80*(34), 4700–4711, doi: 10.1029/JA080i034p04700, 1975.
- 1410 Saito, Y., J. A. Sauvaud, M. Hirahara, S. Barabash, D. Delcourt, T. Takashima, and K. Asamura,
1411 Scientific objectives and instrumentation of Mercury Plasma Particle Experiment (MPPE)
1412 onboard MMO, *Planet. Space Sci.*, *58*(1–2), 182–200, doi: 10.1016/j.pss.2008.06.003,
1413 2010.
- 1414 Saito, Y., M. N. Nishino, M. Fujimoto, T. Yamamoto, S. Yokota, H. Tsunakawa, H. Shibuya,
1415 M. Matsushima, H. Shimizu, and F. Takahashi, Simultaneous observation of the electron
1416 acceleration and ion deceleration over lunar magnetic anomalies, *Earth Planets Space*, *64*,
1417 83–92, doi: 10.5047/eps.2011.07.011, 2012.
- 1418 Sprague, A. L., R. W. H. Kozlowski, D. M. Hunten, W. K. Wells, and F. A. Grosse, The sodium
1419 and potassium atmosphere of the Moon and its interaction with the surface, *Icarus*, *96*(1),
1420 27–42, doi: 10.1016/0019-1035(92)90004-Q, 1992.
- 1421 Stern, S. A., The lunar atmosphere: History, status, current problems, and context, *Rev. Geophys.*,
1422 *37*(4), 453–491, doi: 10.1029/1999RG900005, 1999.
- 1423 Stern, S. A., J. C. Cook, J. Y. Chaufray, P. D. Feldman, G. R. Gladstone, and K. D. Retherford,
1424 Lunar atmospheric H₂ detections by the LAMP UV spectrograph on the Lunar
1425 Reconnaissance Orbiter, *Icarus*, *226*(2), 1210–1213, doi: 10.1016/j.icarus.2013.07.011,
1426 2013.
- 1427 Sternovsky, Z., P. Chamberlin, M. Horanyi, S. Robertson, and X. Wang, Variability of the lunar
1428 photoelectron sheath and dust mobility due to solar activity, *J. Geophys. Res.*, *113*(A10),
1429 doi: 10.1029/2008JA013487, 2008.
- 1430 Stubbs, T. J., R. R. Vondrak, and W. M. Farrell, A dynamic fountain model for lunar dust, *Adv.*
1431 *Space Res.*, *37*(1), 59–66, doi: 10.1016/j.asr.2005.04.048, 2006.
- 1432 Stubbs, T. J., D. A. Glenar, W. M. Farrell, R. R. Vondrak, M. R. Collier, J. S. Halekas, and G. T.
1433 Delory, On the role of dust in the lunar ionosphere, *Planet. Space Sci.*, *59*(13), 1659–1664,
1434 doi: 10.1016/j.pss.2011.05.011, 2011.
- 1435 Sunshine, J. M., T. L. Farnham, L. M. Feaga, O. Groussin, F. Merlin, R. E. Milliken, and M. F.
1436 A'Hearn, Temporal and spatial variability of lunar hydration as observed by the Deep
1437 Impact spacecraft, *Science*, *326*(5952), 565–568, doi: 10.1126/science.1179788, 2009.
- 1438 Szalay, J. R., and M. Horányi, The search for electrostatically lofted grains above the Moon with
1439 the Lunar Dust Experiment, *Geophys. Res. Lett.*, *42*(13), 5141–5146,
1440 doi: 10.1002/2015GL064324, 2015.
- 1441 Taylor, A. D., Earth encounter velocities for interplanetary meteoroids, *Adv. Space Res.*, *17*(12),
1442 205–209, doi: 10.1016/0273-1177(95)00782-A, 1996.
- 1443 Thompson, M., II. the energy spectrum of ejected atoms during the high energy sputtering of
1444 gold, *Philos. Mag.*, *18*, 377–414, doi: 10.1080/14786436808227358, 1968.
- 1445 Tsunakawa, H., F. Takahashi, H. Shimizu, H. Shibuya, and M. Matsushima, Surface vector
1446 mapping of magnetic anomalies over the Moon using Kaguya and Lunar Prospector
1447 observations, *J. Geophys. Res.*, *120*(6), 1160–1185, doi: 10.1002/2014JE004785, 2015.

SELMA: How do airless bodies interact with space environment?

- 1448 Vondrak, R. R., *Lunar base activities and the lunar environment*, vol. 1, pp. 337–345, NASA,
1449 Johnson Space Center, 1983.
- 1450 Vorburgeter, A., P. Wurz, S. Barabash, M. Wieser, Y. Futaana, M. Holmström, A. Bhardwaj, and
1451 K. Asamura, Energetic neutral atom observations of magnetic anomalies on the lunar
1452 surface, *J. Geophys. Res.*, *117*(A7), A07,208, doi: 10.1029/2012JA017553, 2012.
- 1453 Vorburgeter, A., P. Wurz, S. Barabash, M. Wieser, Y. Futaana, C. Lue, M. Holmström, A.
1454 Bhardwaj, M. B. Dhanya, and K. Asamura, Energetic neutral atom imaging of the lunar
1455 surface, *J. Geophys. Res.*, *118*(7), 3937–3945, doi:10.1002/jgra.50337, 2013.
- 1456 Vorburgeter, A., P. Wurz, S. Barabash, M. Wieser, Y. Futaana, M. Holmström, A. Bhardwaj, and
1457 K. Asamura, First direct observation of sputtered lunar oxygen, *J. Geophys. Res.*, *119*(2),
1458 709–722, doi: 10.1002/2013JA019207, 2014.
- 1459 Wang, X., C. T. Howes, M. Horányi, and S. Robertson, Electric potentials in magnetic dipole
1460 fields normal and oblique to a surface in plasma: Understanding the solar wind interaction
1461 with lunar magnetic anomalies, *Geophys. Res. Lett.*, *40*(9), 1686–1690,
1462 doi: 10.1002/grl.50367, 2013.
- 1463 Watson, K., B. C. Murray, and H. Brown, The behavior of volatiles on the lunar surface, *J.*
1464 *Geophys. Res.*, *66*(9), 3033–3045, doi: 10.1029/JZ066i009p03033, 1961.
- 1465 Wieczorek, M. A., B. P. Weiss, and S. T. Stewart, An impactor origin for lunar magnetic
1466 anomalies, *Science*, *335*(6073), 1212–1215, doi: 10.1126/science.1214773, 2012.
- 1467 Wieler, R., K. Kehm, A. P. Meshik, and C. M. Hohenberg, Secular changes in the xenon and
1468 krypton abundances in the solar wind recorded in single lunar grains, *Nature*, *384*(6604),
1469 46–49, doi: 10.1038/384046a0, 1996.
- 1470 Wieser, M., S. Barabash, Y. Futaana, M. Holmström, A. Bhardwaj, R. Sridharan, M. B. Dhanya,
1471 P. Wurz, A. Schaufelberger, and K. Asamura, Extremely high reflection of solar wind
1472 protons as neutral hydrogen atoms from regolith in space, *Planet. Space Sci.*, *57*, 2132–
1473 2134, doi: 10.1016/j.pss.2009.09.012, 2009a.
- 1474 Wieser, M., L. Kalla, S. Barabash, T. Hedqvist, S. Kemi, O. Widell, D. Abplanalp, and P. Wurz,
1475 The Mars Environment Analogue Platform long duration balloon flight, *Adv. Space Res.*,
1476 *44*(3), 308–312, doi: 10.1016/j.asr.2009.03.014, 2009b.
- 1477 Wieser, M., S. Barabash, Y. Futaana, M. Holmström, A. Bhardwaj, R. Sridharan, M. B. Dhanya,
1478 A. Schaufelberger, P. Wurz, and K. Asamura, First observation of a mini-magnetosphere
1479 above a lunar magnetic anomaly using energetic neutral atoms, *Geophys. Res. Lett.*, *37*(5),
1480 doi: 10.1029/2009GL041721, 2010.
- 1481 Wiley, W. C., and I. H. McLaren, Time-of-flight mass spectrometer with improved resolution,
1482 *Rev. Sci. Instrum.*, *26*(12), 1150–1157, doi: 10.1063/1.1715212, 1955.
- 1483 Wilson, J., M. Mendillo, and H. Spence, Magnetospheric influence on the Moon’s exosphere, *J.*
1484 *Geophys. Res.*, *111*(A7), A07,207, doi: 10.1029/2005JA011364, 2006.
- 1485 Wurz, P., U. Rohner, J. A. Whitby, C. Kolb, H. Lammer, P. Dobnikar, and J. A. Martín-
1486 Fernández, The lunar exosphere: The sputtering contribution, *Icarus*, *191*(2), 486–496,
1487 doi: 10.1016/j.icarus.2007.04.034, 2007.
- 1488 Wurz, P., D. Abplanalp, M. Tulej, and H. Lammer, A neutral gas mass spectrometer for the
1489 investigation of lunar volatiles, *Planet. Space Sci.*, *74*(1), 264–269,
1490 doi: 10.1016/j.pss.2012.05.016, 2012.
- 1491 Yokota, S., and Y. Saito, Estimation of picked-up lunar ions for future compositional remote
1492 SIMS analyses of the lunar surface, *Earth Planets Space*, *57*, 281–289,
1493 doi: 10.1186/BF03352564, 2005.
- 1494 Yurimoto, H., K. Kuramoto, A. N. Krot, E. R. D. Scott, J. N. Cuzzi, M. H. Thieme, and J. R.
1495 Lyons, Origin and evolution of oxygen-isotopic compositions of the solar system, in
1496 *Protostars and Planets V*, edited by B. Reipurth, D. Jewitt, and K. Keil, pp. 849–862,
1497 University of Arizona Press, Tucson, 2007.

SELMA: How do airless bodies interact with space environment?

1498 Zimmerman, M. I., W. M. Farrell, and A. R. Poppe, Kinetic simulations of kilometer-scale mini-
1499 magnetosphere formation on the Moon, *J. Geophys. Res.*, 120(11), 1893–1903,
1500 doi: 10.1002/2015JE004865, 2015.

1501 Zook, H. A., and J. E. McCoy, Large scale lunar horizon glow and a high altitude lunar dust
1502 exosphere, *Geophys. Res. Lett.*, 18(11), 2117, doi: 10.1029/91GL02235, 1991.

1503

1504 **Appendix A: SELMA proposal team members**

1505 The SELMA mission was proposed to ESA in response to the call for the medium-size mission
1506 opportunity (M5). The proposal team members are listed below.

1507 **Lead proposer:** Stas Barabash (Swedish Institute of Space Physics, Kiruna, Sweden)

1508 **Science lead:** Yoshifumi Futaana (Swedish Institute of Space Physics, Kiruna, Sweden)

1509 **Principal Investigators:**

1510 Peter Wurz (University of Bern, Bern, Switzerland)

1511 Mihaly Horanyi (Laboratory for Atmospheric and Space Physics, University of Colorado, USA)

1512 Urs Mall (Max Planck Institute for Solar System Research, Göttingen, Germany)

1513 Martin Wieser (Swedish Institute of Space Physics, Kiruna, Sweden)

1514 Nicolas Andre (IRAP- Université de Toulouse, CNRS, France)

1515 Nickolay Ivchenko (KTH Royal Institute of Technology, Stockholm, Sweden)

1516 Jürgen Oberst (German Aerospace Center, Berlin, Germany)

1517 Kurt Retherford (Southwest Research Institute, San Antonio, USA)

1518 Andrew Coates (Mullard Space Science Laboratory, University College London, London, UK)

1519 Adam Masters (Imperial College London, London, UK)

1520 Jan-Erik Wahlund (Swedish Institute of Space Physics, Uppsala, Sweden)

1521 Esa Kallio (Aalto University, Helsinki, Finland)

1522 **Co-Investigators:**

1523 M. Holmström, X.-D. Wang, G. Nicolaou, G. S. Wieser, H. Nilsson, S. Fatemi (Swedish Institute
1524 of Space Physics, Kiruna, Sweden); A. Vorburger (University of Bern, Bern, Switzerland); A.
1525 Fedorov (IRAP, Toulouse, France); A. Margonis, S. Elgner (DLR, Berlin, Germany); J. Bergman,
1526 D. Andrews, M. André, S. Buchert, M. Morooka, N. Edberg, A. Eriksson (Swedish Institute of
1527 Space Physics, Uppsala, Sweden); Z. Sternovsky, J. Deca (Laboratory for Atmospheric and
1528 Space Physics, University of Colorado, USA), J. Szalay (Southwest Research Institute, San
1529 Antonio, USA); W. Schmidt (Finnish Meteorological Institute, Helsinki, Finland); Charles Lue
1530 (Department of Physics and Astronomy, University of Iowa, USA); O. Korablev, A. Ivanov, A.
1531 Fedorova, R. Kuzmin; V. Izmodenov (Space Research Institute, Moscow, Russia); C. M. Pieters
1532 (Brown University, Providence, Rhode Island, USA); K. Szego, S. Sandor, Z. Nemeth (Wigner
1533 Research Centre for Physics, Institute for Particle and Nuclear Physics, Budapest, Hungary); R.
1534 Green (Jet Propulsion Laboratory, Pasadena, California, USA); R. C. Clark (US Geological
1535 Survey, Denver, Colorado, USA); M. Banaszkiwicz M. Bzowski (Space Research Center,
1536 Warsaw, Poland); L. Roth (Royal Institute of Technology, Stockholm, Sweden); I. Mann
1537 (EISCAT scientific association, Kiruna, Sweden); K. Dhiren (Mullard Space Science Laboratory,

SELMA: How do airless bodies interact with space environment?

1538 University College London, London, UK); M. Grande (Aberystwyth University, UK); D. Hurley
1539 (The Johns Hopkins University Applied Physics Laboratory, Laurel, USA).

1540